ISSN 0280–5316
ISRN LUTFD2/TFRT--5563--SE

The Effect of Friction on Stabilization of an Inverted Pendulum

Carl Fredrik Abelson

Department of Automatic Control
Lund Institute of Technology
September 1996

Department of Automatic Control
Lund Institute of Technology
Box 118
S-221 00 Lund Sweden

Document name
Master Thesis

Date of issue
September 1996

Document Number
ISRN LUTFD2/TFRT--5563--SE

Author(s)
Carl Fredrik Abelson

Supervisor
Henrik Olsson
Karl Johan Åström

Sponsoring organisation

Title and subtitle
The Effect of Friction on Stabilization of an Inverted Pendulum

Abstract

This thesis investigates frictional effects on the stabilization of a rotating inverted pendulum. Because of friction, limit cycles arise when trying to stabilize the inverted pendulum. The stabilization is done using linear state feedback. For estimation of the states, Kalman filters are used. Both real-time experiments and simulations are performed.

Two friction models are used, one classical with stiction and Coulomb friction, and one advanced and dynamic, the LuGre model. These are identified by comparing limit cycles from the real process with limit cycles obtained through simulations. Since the inverted pendulum is an unstable process with fast dynamics, it is sensitive to parameter changes, and thus it is difficult to get good results. Model-based friction compensation is also tried. This results in reduced limit cycles.

Key words
Inverted Pendulum, Friction, Limit Cycles, Friction Identification, Friction Compensation, LuGre Model

Classification system and/or index terms (if any)

Supplementary bibliographical information

ISSN and key title
0280–5316

ISBN

Language
English

Number of pages
66

Recipient's notes

Security classification

Preface

In order to become Master of Science one has to do a Master Thesis Project. This report describes the project I did. It was done during the spring and summer of 1996 at the Department of Automatic Control of Lund Institute of Technology.

In order to explain why I choose the present subject we have to go back to the fall of 1995. At that time I took a course in Real Time Systems and in order to pass it, one were required to do a project. I choose to implement a regulator for an inverted pendulum. The report for that project is Abelson *et al.* (1995). Earlier this spring I took a course called System Identification. In this, it was also required to do a project. Since I had become fascinated by the inverted pendulum during the project in Real Time Systems, I choose it for the system to identify. The result was Abelson and Christelius (1996).

After having done two projects on the inverted pendulum I had got quite a good knowledge of it. I therefore thought that it would be a good idea to deepen this knowledge by doing my Master Thesis project on it.

As supervisors for the project I had Karl Johan Åström, who is the Professor at the department, and Henrik Olsson, who finished his PhD during the time I did my thesis. I would like to express my gratitude to them for supporting me and for giving me good advices. Thank you! Also, I should thank Mikael Johansson for giving me a copy of an old project report in Real Time Systems on the inverted pendulum. Johan Eker supplied me with a copy of Eker *et al.* (1996), a mathematical model of the inverted pendulum on which parts of Section 2.1 in this report is based, and Eker and Åström (1996), a description of a nonlinear observer for the inverted pendulum. He also gave me a copy of a PAL-program for swinging up and regulating the pendulum. Thank you two!

Let's end the preface with a joke! I have a habit of first writing my reports using pencil and paper and then afterwards type them into the computer. Typing is very mechanical. Applying the syllogism in the beginning of Section 1 means that there was friction while typing. Indeed there was!

Lund, July 1996

Carl Fredrik Abelson

Contents

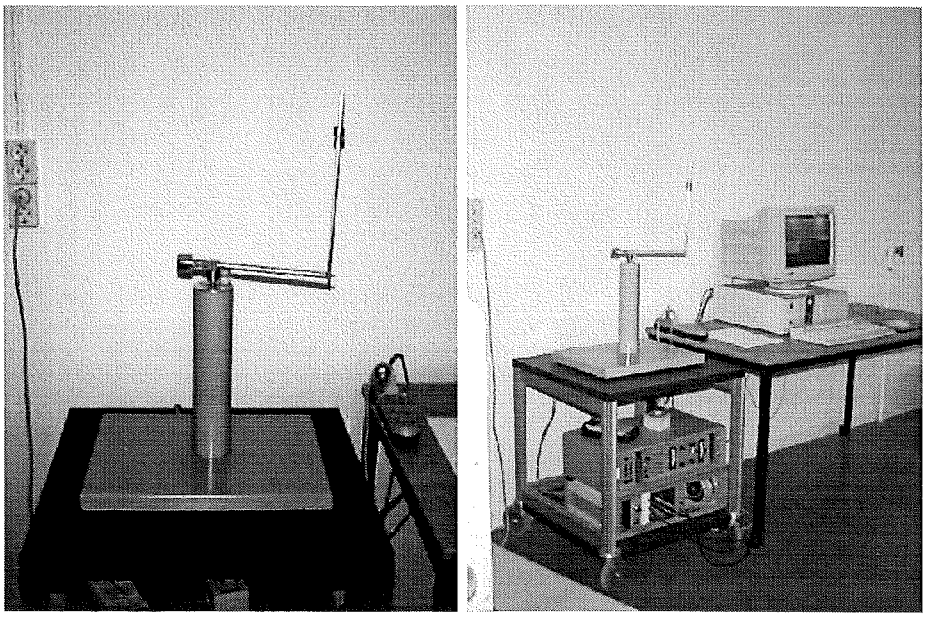

Figure 1 The inverted pendulum, and the pendulum plus the real-time computer.

1. Introduction

This report has two subjects, the inverted pendulum and friction. Somewhat simplified and humorous, the connection between these can be made by the following syllogism. Friction exists in every mechanical system. The inverted pendulum is a mechanical system. Therefore, friction is affecting the inverted pendulum.

The inverted pendulum is an unstable process. It consists of a pendulum which is to be balanced. There are many kinds of inverted pendulums. The one used in this project may be described as follows. An arm is mounted to a center pillar, and a pendulum is attached to the arm. Both the arm and the pendulum may be rotated. The acceleration of the arm may be controlled. A photo of the inverted pendulum is in Figure 1.

Friction may occur in two places. The first is in the bearing by which the arm is mounted to the center pillar, and the second is in the bearing which connects the pendulum to the arm. In this project, it is assumed that the latter friction is negligible and thus only the former will be examined. Except for the bearing, this friction is explained by three contact pins. They are used to transmit the measurements of the pendulum position, the arm position and the arm velocity.

When trying to control the inverted pendulum with a simple, linear controller one gets limit cycles because of the friction. The size and shape of these depend on the nature of the friction. Therefore, the limit cycles may be used to determine suitable parameters for a friction model, e.g., by simulation. A description of this, along with results from such investigations, is presented in this report. The size of the friction has also been determined using simpler methods. Also, it has been examined if the friction differs for different directions of the arm.

Friction is a very simple or a very complicated phenomenon, depending on how accurately one looks at it. On a macroscopic, or rough, level it is

easy to understand but on a detailed level there are a number of peculiarities associated with it. Because of this, there is an abundance of friction models, reaching from simple ones with a single parameter to differential equations of high order and with many parameters. In this thesis two models have been used, a simple one and an advanced one. Parameters for both models have been identified and their performances have been compared. It has been examined how much better the advanced model is in capturing the friction of the inverted pendulum. Both models, along with some properties of friction, are presented in Section 3.

Before closing this section, the outline for the rest of the report is presented. The report consists of three parts followed by a summary. In the first part the theoretical background is presented. Section 2 contains a presentation of the inverted pendulum. A mathematical model is derived and the linear controller used to control it is described. Section 3 is about friction. Some basic properties are presented along with the two friction models used in the experiments. Limit cycles is the theme of Section 4. Some methods for predicting them are given along with their relationship with friction.

Sections 5 and 6 make up the experimental part. In these, the practical experiments are presented. Section 5 gives the results from simulation experiments of the friction models. In Section 6, model-based friction compensation is tried.

In order to perform many of the tests on the real process, a real-time regulator had to be written. This is presented in Section 7. A user's guide is given and the internal structure of the program is presented.

The last section consists of a summary of the report followed by some concluding remarks. Possible extensions of the thesis are also mentioned.

2. The Inverted Pendulum

The inverted pendulum is a common example of an unstable process. This is partly explained by the fact that such a device is fairly easy to construct. The pendulum used in this project was built at the Department of Automatic Control at Lund Institute of Technology in Lund, Sweden.

It is pictured in Figure 1. It consists of a pendulum, an arm and a center pillar. The arm is mounted on the center pillar and may be rotated in a horizontal plane. The pendulum is attached to the arm and it may also be rotated, but in a vertical plane. The point where the pendulum is attached to the arm is called the *pivot point.*

The process has two equilibrium points. The downward position corresponds to an ordinary pendulum. This point is stable and in the phase plane it has the character of a stable node. The upright, or inverted, position is unstable and has the character of a saddle point. The goal is to design a regulator so that the upper equilibrium point in the closed loop system is stable. In other words, the pendulum should be balanced.

Three signals can be measured. The angle and the velocity of the arm, and the angle of the pendulum. The input to the process is the voltage to the motor. This is approximately proportional to the acceleration of the arm.

2.1 Mathematical Models

In this subsection a nonlinear model of the inverted pendulum will be derived. The derivation is based on Eker *et al.* (1996).

The angle of the arm in radians is denoted by Ω and the angle of the pendulum, also in radians, is denoted by θ. The angle $\theta = 0$ means a pendulum in its upright position.

The dynamics of the drive electronics are fast and can be neglected. The input voltage thus results in a torque on the arm. The relation between the control voltage V and the angular acceleration of the arm $\ddot{\Omega}$ can be described by the following proportionality:

$$J\ddot{\Omega} = kV$$

Choose as the theoretical control signal u the acceleration of the arm in $\mathrm{m/s^2}$. The relation between u and $\ddot{\Omega}$ is

$$u = \ddot{\Omega} L_1 \tag{1}$$

where L_1 is the length of the arm.

It is assumed that the arm is weightless and that the mass of the pendulum is concentrated to a single point, the mass point.

The model is derived using a force equation. Before stating it, the acceleration of the mass point is calculated. Two coordinate systems are used, a rotating coordinate system $(\vec{e_1}\vec{e_2}\vec{e_3})$ and a static coordinate system $(\vec{e_1^*}\vec{e_2^*}\vec{e_3^*})$ The base vectors are defined in Figure 2. The relationship between the coordinate systems may be described by a rotational transformation.

$$\begin{pmatrix} \vec{e_1} & \vec{e_2} & \vec{e_3} \end{pmatrix} = \begin{pmatrix} \vec{e_1^*} & \vec{e_2^*} & \vec{e_3^*} \end{pmatrix} \begin{pmatrix} \cos\Omega & -\sin\Omega & 0 \\ \sin\Omega & \cos\Omega & 0 \\ 0 & 0 & 1 \end{pmatrix}$$

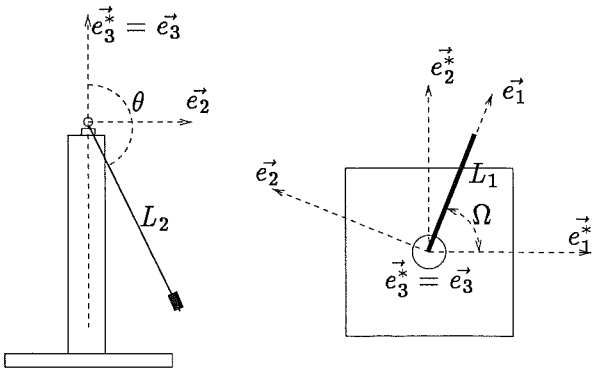

Figure 2 The coordinate systems used in the derivation. L_1 denotes the length of the arm, and L_2 denotes the length of the pendulum.

Let $\vec{r}$ be a vector that points at the mass point. An expression for it in the rotating coordinate system can be calculated using some trigonometry.

$$(\vec{r})_{\vec{e}} = \begin{pmatrix} L_1 & L_2\sin(\theta) & L_2\cos(\theta) \end{pmatrix}$$

The velocity of the mass point is calculated by taking the time derivative of $(\vec{r})_{\vec{e}}$.

$$(\vec{v})_{\vec{e}} = (\dot{\vec{r}})_{\vec{e}} = \begin{pmatrix} 0 & L_2\cos(\theta)\dot{\theta} & -L_2\sin(\theta)\dot{\theta} \end{pmatrix}$$

The acceleration is obtained in a corresponding way.

$$(\vec{a})_{\vec{e}} = (\dot{\vec{v}})_{\vec{e}} = \begin{pmatrix} 0 & L_2(\cos(\theta)\ddot{\theta} - \sin(\theta)(\dot{\theta})^2) & -L_2(\sin(\theta)\ddot{\theta} + \cos(\theta)(\dot{\theta})^2) \end{pmatrix}$$

The axis of rotation is $\vec{e_3} = \vec{e_3^*}$. This is a static axis and common for both coordinate systems. In vector form, the angular velocity $\vec{\omega}$ and the angular acceleration $\vec{\alpha}$ may therefore be expressed as follows:

$$(\vec{\omega})_{\vec{e}} = (\vec{\omega})_{\vec{e}^*} = \dot{\Omega} \cdot \vec{e_3}$$
$$(\vec{\alpha})_{\vec{e}} = (\vec{\alpha})_{\vec{e}^*} = \dot{\vec{\omega}} = \ddot{\Omega} \cdot \vec{e_3}$$

The wanted acceleration is the one in the static coordinate system, not the one in the rotating coordinate system. Using a standard mechanics theorem, the relation between the two accelerations may be expressed as:

$$\vec{a^*} = \vec{\alpha} \times \vec{r} + \vec{\omega} \times (\vec{\omega} \times \vec{r}) + 2\vec{\omega} \times \vec{v} + \vec{a}$$

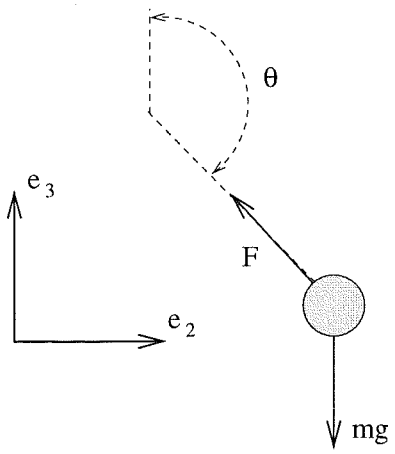

Figure 3 The forces acting on the mass point.

Inserting the above expressions gives

$$\begin{aligned}
\vec{a^*} = &\begin{pmatrix} 0 & 0 & \ddot{\Omega} \end{pmatrix} \times \begin{pmatrix} L_1 & L_2 \sin\theta & L_2 \cos\theta \end{pmatrix} + \\
&\begin{pmatrix} 0 & 0 & \dot{\Omega} \end{pmatrix} \times \left(\begin{pmatrix} 0 & 0 & \dot{\Omega} \end{pmatrix} \times \begin{pmatrix} L_1 & L_2 \sin\theta & L_2 \cos\theta \end{pmatrix} \right) + \\
&2 \begin{pmatrix} 0 & 0 & \dot{\Omega} \end{pmatrix} \times \begin{pmatrix} 0 & L_2 \cos(\theta)\dot{\theta} & -L_2 \sin(\theta)\dot{\theta} \end{pmatrix} + \\
&\begin{pmatrix} 0 & L_2(\cos(\theta)\ddot{\theta} - \sin(\theta)\dot{\theta}^2 & -L_2(\sin(\theta)\ddot{\theta} + \cos(\theta)\dot{\theta}^2 \end{pmatrix} = \\
&\begin{pmatrix} -\ddot{\Omega} L_2 \sin\theta & \ddot{\Omega} L_1 & 0 \end{pmatrix} + \begin{pmatrix} -\dot{\Omega}^2 L_1 & -\dot{\Omega}^2 L_2 \sin\theta & 0 \end{pmatrix} + \\
&2 \begin{pmatrix} -\dot{\Omega}\dot{\theta} L_2 \cos\theta & 0 & 0 \end{pmatrix} + \\
&\begin{pmatrix} 0 & L_2(\cos\theta\ddot{\theta} - \sin\theta\dot{\theta}^2) & -L_2(\sin\theta\ddot{\theta} + \cos\theta\dot{\theta}^2) \end{pmatrix} = \\
&\begin{pmatrix} a_1 & a_2 & a_3 \end{pmatrix}
\end{aligned}$$

where

$$\begin{cases} a_1 = -\ddot{\Omega} L_2 \sin\theta - \dot{\Omega}^2 L_1 - 2\dot{\Omega}\dot{\theta} L_2 \cos\theta \\ a_2 = \ddot{\Omega} L_1 - \dot{\Omega}^2 L_2 \sin\theta + L_2(\cos\theta\ddot{\theta} - \sin\theta\dot{\theta}^2) \\ a_3 = -L_2(\sin\theta\ddot{\theta} + \cos\theta\dot{\theta}^2) \end{cases}$$

A force equation is now stated. It is assumed that only two forces act on the mass point, gravity and the tension in the pendulum. Figure 3 shows these forces. The force equation is stated in vector form with one equation per axis. The forces have no composant in the e_1-axis, resulting in only two equations. They were derived using Figure 3 and trigonometry.

$$\begin{cases} ma_2 = -F \sin\theta \\ ma_3 = -F \cos\theta - mg \end{cases}$$

Eliminating F yields

$$ma_2 \cos\theta - ma_3 \sin\theta - mg \sin\theta = 0$$

Insert the expressions for a_2 and a_3 and simplify.

$$\ddot{\Omega} L_1 \cos\theta - \dot{\Omega}^2 L_2 \sin\theta \cos\theta + L_2 \ddot{\theta} - g \sin\theta = 0 \tag{2}$$

Introduce the resonance frequency of the pendulum ω_0.

$$\omega_0 = \sqrt{\frac{g}{L_2}}$$

Inserting this and the expression for the control signal (1) in (2) gives a model of the inverted pendulum.

$$\begin{cases} \ddot{\theta} = \omega_0^2 \sin\theta + \dot{\Omega}^2 \sin\theta \cos\theta - \dfrac{\omega_0^2 u}{g} \cos\theta \\ \ddot{\Omega} = \dfrac{u}{L_1} \end{cases} \tag{3}$$

The term $\dot{\Omega}^2 \sin\theta \cos\theta$ is due to the centripetal force.

Damping. In the above derivation, damping was not considered. The oscillations of the pendulum are damped, see for example Figure 33 in Appendix A. Introduction of a linear damping term $-2\zeta\omega_0\dot{\theta}$ gives

$$\begin{cases} \ddot{\theta} = -2\zeta\omega_0\dot{\theta} + \omega_0^2 \sin\theta + \dot{\Omega}^2 \sin\theta \cos\theta - \dfrac{\omega_0^2 u}{g} \cos\theta \\ \ddot{\Omega} = \dfrac{u}{L_1} \end{cases} \tag{4}$$

Friction. Friction is affecting the arm. Therefore a friction term is introduced. Denote the friction force by F_{fr} and the actual acceleration of the arm by a. A force equation for the arm may then be stated.

$$ma = mu - F_{fr}$$

Introduce $a = \ddot{\Omega} L_1$ and solve for $\ddot{\Omega}$.

$$\ddot{\Omega} = \frac{u}{L_1} - \frac{F_{fr}}{m} \frac{1}{L_1} \tag{5}$$

Inserting this expression into (4) gives the following model:

$$\begin{cases} \ddot{\theta} = -2\zeta\omega_0\dot{\theta} + \omega_0^2 \sin\theta + \dot{\Omega}^2 \sin\theta \cos\theta - \dfrac{\omega_0^2 u}{g} \cos\theta + \dfrac{F_{fr}}{m} \dfrac{\omega_0^2}{g} \cos\theta \\ \ddot{\Omega} = \dfrac{u}{L_1} - \dfrac{F_{fr}}{m} \dfrac{1}{L_1} \end{cases} \tag{6}$$

Model Parameters. The model has three parameters that have to be identified. This is done in Appendix A. The following values resulted

$$\begin{cases} \omega_0 = 6.8 \text{ rad/s} \\ \zeta = 0.04 \\ L_1 = 0.21 \text{ m} \end{cases}$$

Determination of the friction force F_{fr} is the subject of this thesis. Models for it will be given in later sections.

Conversion Factors. In the equations above, variables in SI units are used. These theoretical variables differ from the signals sent to and received from the real process. The latter ones are scaled and biased voltages. Since it is desirable to use SI units inside the regulator, these voltages should be converted to such after having been read from the ADC, or before being sent to the DAC. Conversion factors for doing this are determined in Appendix B.

Denote the measured angle of the arm by x, the measured velocity of the arm by v and the measured angle of the pendulum by y. Further, denote the control signal sent to the DAC by u_{DA}. Then the conversion formulas between the measured and the theoretical signals are

$$\begin{cases} \theta = \pi(y + 0.503) & y \in [-1, 1] \\ \Omega = 25.8(x - x_0) & x \in [-1, 1] \\ \dot{\Omega} = 28.7(v + 0.02) & v \in [-1, 1] \\ u_{DA} = -0.022u & u_{DA} \in [-1, 1] \end{cases}$$

2.2 State Feedback

The inverted pendulum is not stable. In order to stabilize it, it must be connected to a regulator. The control strategy chosen is linear state feedback. It is not the control that gives the best performance, but it is simple and it gives good performance. Since a real-time computer will be used to implement the controller, it is designed in discrete-time. The control law has the following form:

$$u(k) = -Lx(k)$$

where

$$L = \begin{bmatrix} l_1 & l_2 & l_3 & l_4 \end{bmatrix}$$

Friction and damping are neglected, therefore the model (3) is used. In order to do a design using linear techniques, this model is linearized. Introduction of the state vector

$$x = \begin{bmatrix} \theta \\ \dot{\theta} \\ \Omega \\ \dot{\Omega} \end{bmatrix}$$

and linearization around the upright position, i.e., $x = \begin{bmatrix} 0 & 0 & 0 & 0 \end{bmatrix}^T$ gives the system

$$\begin{cases} \dfrac{dx}{dt} = \begin{bmatrix} 0 & 1 & 0 & 0 \\ \omega_0^2 & 0 & 0 & 0 \\ 0 & 0 & 0 & 1 \\ 0 & 0 & 0 & 0 \end{bmatrix} x + \begin{bmatrix} 0 \\ -\frac{\omega_0^2}{g} \\ 0 \\ 1/L_1 \end{bmatrix} u \\ y = \begin{bmatrix} 1 & 0 & 0 & 0 \\ 0 & 0 & 1 & 0 \\ 0 & 0 & 0 & 1 \end{bmatrix} x \end{cases} \tag{7}$$

Since the controller will be implemented in discrete-time, the system must be discretized. Using standard methods[1] the following discrete-time version of (7) is obtained:

$$\begin{cases} x(k+1) = \Phi x(k) + \Gamma u(k) \\ y(k) = Cx(k) \end{cases}$$

where

$$\Phi = \begin{bmatrix} \cosh(\omega_0 h) & \frac{1}{\omega_0}\sinh(\omega_0 h) & 0 & 0 \\ \omega_0 \sinh(\omega_0 h) & \cosh(\omega_0 h) & 0 & 0 \\ 0 & 0 & 1 & h \\ 0 & 0 & 0 & 1 \end{bmatrix}$$

and

$$\Gamma = \begin{bmatrix} -\frac{1}{g}(\cosh(\omega_0 h) - 1) \\ -\frac{\omega_0}{g}\sinh(\omega_0 h) \\ \frac{h^2}{2L_1} \\ h/L_1 \end{bmatrix}$$

The specifications for the regulator are given in continuous time. Assume that the desired characteristic equation is

$$(s^2 + 2\zeta_1\omega_1 s + \omega_1^2)(s^2 + 2\zeta_2\omega_2 s + \omega_2^2) = 0.$$

The denotations ω_1 and ζ_1 stand for the desired natural frequency and damping of the pendulum, and ω_2 and ζ_2 stand for the ditto of the arm. The corresponding discrete-time equation is

$$(q^2 + p_1 q + p_2)(q^2 + p_3 q + p_4) = 0 \tag{8}$$

where

$$\begin{cases} p_1 = -2e^{-\omega_1\zeta_1 h}\cos(\omega_1\sqrt{1-\zeta_1^2}h) \\ p_2 = e^{-2\omega_1\zeta_1 h} \\ p_3 = -2e^{-\omega_2\zeta_2 h}\cos(\omega_2\sqrt{1-\zeta_2^2}h) \\ p_4 = e^{-2\omega_2\zeta_2 h} \end{cases}$$

The characteristic equation for the closed loop system is

$$\det(qI - (\Phi - \Gamma L)) = 0 \tag{9}$$

By setting the characteristic equations (8) and (9) equal and solving for L, one gets expressions for the regulator parameters. Unfortunately these are large, and they are therefore not given here. The interested reader may find them in Appendix C.

Before being able to calculate the L-vector another parameter has to be set, namely the sampling period h. Since the inverted pendulum is an unstable process with fast dynamics, this should be chosen as small as possible. In this thesis, the following value was used:

$$h = 0.005 \text{ s}$$

[1] See for example Section 3.2 in Åström and Wittenmark (1990).

2.3 Observers

Only three out of the four states are measureable. The fourth, the velocity of the pendulum, has to be estimated. The measurements are a bit noisy. If the control signal is calculated using them, this also gets noisy. Therefore, all states should be estimated, and the estimates should be used to calculate the control signal. For the estimation, Kalman filters were used.

A Nonlinear Kalman Filter for the Pendulum. The pendulum is a nonlinear process. This can be seen in, for example, Eq. (3). For high precision, a nonlinear estimator is therefore preferred. A Kalman filter is used. The following presentation is partly based on Eker and Åström (1996). The major difference is that the centripetal term $\dot{\Omega}^2 \sin\theta \cos\theta$ has been included in the Kalman filter. The reason is that the performance of the real inverted pendulum may be increased, since larger deviations of the arm position can be tolerated.

For simplicity, damping is disregarded. The remaining pendulum equation is

$$\ddot{\theta} = \omega_0^2 \sin\theta + \dot{\Omega}^2 \sin\theta \cos\theta - \frac{\omega_0^2 u}{g} \cos\theta$$

Introduce the following state variables

$$\begin{cases} x_1 = \theta \\ x_2 = \dfrac{1}{\omega_0}\dot{\theta} \end{cases}$$

The system then becomes

$$\begin{cases} \dfrac{dx_1}{dt} = \omega_0 x_2 \\ \dfrac{dx_2}{dt} = \omega_0 \sin x_1 + \dot{\Omega}^2 \sin x_1 \cos x_1 - \dfrac{\omega_0 u}{g} \cos x_1 \end{cases} \tag{10}$$

As with linear Kalman filters, a nonlinear filter is obtained by replacing the states with their estimated counterparts plus adding correction terms to both state equations. The measurable signal is the pendulum angle $\theta = x_1$.

$$\begin{cases} \dfrac{d\hat{x}_1}{dt} = \omega_0 \hat{x}_2 + k_1(x_1 - \hat{x}_1) \\ \dfrac{d\hat{x}_2}{dt} = \omega_0 \sin\hat{x}_1 - \hat{\dot{\Omega}}^2 \sin\hat{x}_1 \cos\hat{x}_1 + \dfrac{\omega_0 u}{g} \cos\hat{x}_1 + k_2(x_1 - \hat{x}_1) \end{cases}$$

The filter gains are calculated using linearization. No swingup is implemented, so the system is linearized around the upright position $x = (0, 0)$ and $\dot{\Omega} = 0$. With $\dot{\Omega} = 0$, the system matrix of (10) is

$$f(x_1, x_2) = \begin{bmatrix} \omega_0 x_2 \\ \omega_0 \sin x_1 \end{bmatrix}$$

The Jacobian is calculated for the upright position.

$$A = \frac{\partial f}{\partial x} = \begin{bmatrix} 0 & \omega_0 \\ \omega_0 & 0 \end{bmatrix}$$

The characteristic polynomial of the Kalman filter may now be calculated. Since the pendulum angle is measurable, C=[1 0].

$$\det(sI-(A-KC)) = \begin{vmatrix} s+k_1 & -\omega_0 \\ k_2-\omega_0 & s \end{vmatrix} = s^2 + k_1 s + \omega_0(k_2-\omega_0)$$

Assume that the desired characteristic polynomial is

$$s^2 + 2\zeta_{o1}\omega_{o1}s + \omega_{o1}^2$$

By identification of coefficients, expressions for the filter gains can be given.

$$\begin{cases} k_1 = 2\zeta_{o1}\omega_{o1} \\ k_2 = \dfrac{\omega_{o1}^2}{\omega_0} + \omega_0 \end{cases}$$

The stability of the Kalman filter has not been investigated. In simulations and in practical tests, it has however been found to be stable. Stability of a Kalman filter without the centripetal term and with general filter gains is studied in Eker and Åström (1996).

The Kalman filter was implemented using a real-time computer. Since it is nonlinear, it is difficult to discretize. Therefore, it was implemented using finite differences to approximate the derivatives.

A Linear Kalman Filter for the Arm. The arm is modelled by a linear double integrator, and thus it suffices with a linear Kalman filter. A discrete-time filter is used.

Introduce the state vector

$$x_2 = \begin{bmatrix} \Omega \\ \dot{\Omega} \end{bmatrix}$$

The subsystem for the arm may then be written

$$\begin{cases} x_2(k+1) = \Phi_2 x_2(k) + \Gamma_2 u(k) \\ y_2(k) = C_2 x_2(k) \end{cases}$$

where

$$\Phi_2 = \begin{bmatrix} 1 & h \\ 0 & 1 \end{bmatrix}$$

$$\Gamma_2 = \begin{bmatrix} \frac{1}{2}\frac{h^2}{L_1} \\ h/L_1 \end{bmatrix}$$

$$C_2 = [1 \quad 0]$$

The Kalman filter is created by replacing x_2 and y_2 with their estimated counterparts, $\hat{x}_2$ and $\hat{y}_2$, and by adding a correction term to the state equation.

$$\begin{cases} \hat{x}_2(k+1) = \Phi_2 \hat{x}_2(k) + \Gamma_2 u(k) + K_2(y_2 - C_2 \hat{x}_2(k)) \\ \hat{y}_2(k) = C_2 \hat{x}_2(k) \end{cases}$$

Expressions for the gain vector $K_2 = [\, k_3 \quad k_4 \,]^T$ are now calculated. Continuous time specifications are used. Introduce the desired characteristic equation

$$s^2 + 2\zeta_{o2}\omega_{o2}s + \omega_{o2}^2 = 0$$

where ω_{o2} is the desired natural frequency and ζ_{o2} is the desired damping. The discrete-time counterpart is

$$q^2 + p_{o3}q + p_{o4} = 0 \tag{11}$$

where

$$\begin{cases} p_{o3} = -2e^{-\omega_{o2}\zeta_{o2}h}\cos(\omega_{o2}\sqrt{1-\zeta_{o2}^2}h) \\ p_{o4} = e^{-2\omega_{o2}\zeta_{o2}h} \end{cases}$$

The characteristic equation for the Kalman filter is

$$\det(qI - (\Phi_2 - K_2 C_2)) = 0 \tag{12}$$

By setting (11) and (12) equal and solving for K_2 one gets the following expressions for the filter gains

$$\begin{cases} k_3 = 2 + p_{o3} \\ k_4 = \dfrac{1 + p_{o3} + p_{o4}}{h} \end{cases}$$

2.4 Controller Parameters

In the experiments, two control designs are used. In the first the control of the arm is faster than the control of the pendulum. Its state feedback specifications are

$$\begin{cases} \omega_1 = \omega_0 = 6.8 \\ \zeta_1 = 0.7 \\ \omega_2 = 10 \\ \zeta_2 = 0.7 \end{cases} \tag{13}$$

and its Kalman filter specifications are

$$\begin{cases} \omega_{o1} = 20 \\ \zeta_{o1} = 0.7 \\ \omega_{o2} = 10 \\ \zeta_{o2} = 0.7 \end{cases} \tag{14}$$

In the second design, the control of the arm is slower than the control of the pendulum. Its specifications are

$$\begin{cases} \omega_1 = \omega_0 = 6.8 \\ \zeta_1 = 0.7 \\ \omega_2 = 3 \\ \zeta_2 = 0.7 \end{cases} \tag{15}$$

and

$$\begin{cases} \omega_{o1} = 20 \\ \zeta_{o1} = 0.7 \\ \omega_{o2} = 7.5 \\ \zeta_{o2} = 0.7 \end{cases} \tag{16}$$

The gains for the state feedback loop and for the Kalman filters corresponding to these control specifications are given in Appendix D.

The bandwidth for the pendulum, ω_1, is chosen the same as its resonance frequency ω_0. The choice of 10 and 3 for ω_2 is arbitrary, the first is higher than ω_1 and the second is lower. The Kalman filter for the pendulum is faster than the state feedback, about three times. The Kalman filter for the arm in the case of the slow design is 2.5 times faster than the state feedback. For the fast design they have the same bandwidth. The latter was optimized experimentally. The dampings are all set to the standard value of 0.7.

2.5 Summary

The inverted pendulum was the subject of this section. A nonlinear process model was derived, and model parameters were given. Further, a friction term was introduced. The result was the following process model:

$$\begin{cases} \ddot{\theta} = -2\zeta\omega_0\dot{\theta} + \omega_0^2 \sin\theta + \dot{\Omega}^2 \sin\theta\cos\theta - \dfrac{\omega_0^2 u}{g}\cos\theta + \dfrac{F_{fr}}{m}\dfrac{\omega_0^2}{g}\cos\theta \\ \ddot{\Omega} = \dfrac{u}{L_1} - \dfrac{F_{fr}}{m}\dfrac{1}{L_1} \end{cases}$$

where

$$\begin{cases} \omega_0 = 6.8 \text{ rad/s} \\ \zeta = 0.04 \\ L_1 = 0.21 \text{ m} \end{cases}$$

To control the inverted pendulum, linear state feedback is used. To estimate the position and the velocity of the pendulum, a nonlinear Kalman filter is used, to estimate ditto for the arm, a linear Kalman filter is used. In the practical experiments, two control designs are used, one with fast control of the arm, and one with slow control of the arm.

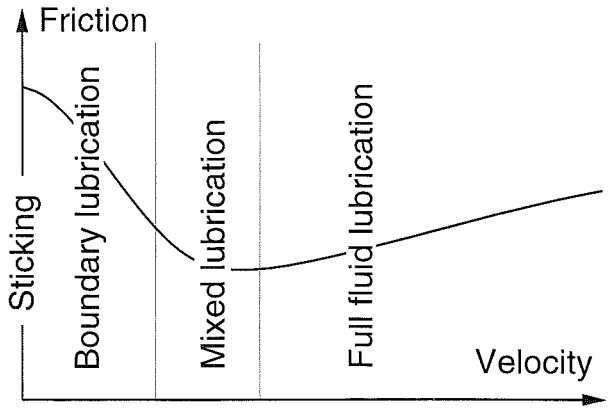

Figure 4 Stribeck curve. Friction may be divided into four regions depending on the origin of the friction.

3. Friction

In the introductory courses in physics[2] friction is taught only rudimentarily. One usually learns only of its existence, that it opposes motion and that there are two kinds of friction, one during zero velocity and one during motion. Friction force is usually described by

$$F = \mu N$$

where N is the normal force and μ is the coefficient of friction. There are two kinds of μ, the *coefficient of static friction* μ_s and the *coefficient of kinetic friction* μ_k.

The friction model described above is good for a general understanding of friction and for simple, classroom experiments. If one requires deeper understanding of friction, more advanced models are required. In this section such models are given. Also further properties of friction will be given. This section is based on Chapters 2 and 3 in Olsson (1996). For a more detailed presentation of friction, these are recommended. They also give a few more of the vast number of friction models.

3.1 Some Basic Properties

In the introductory courses it is assumed that the kinetic friction is the same for all velocities. This is a simplification since the friction force varies with velocity. The relation may look as in Figure 4. This is called a *Stribeck curve* after R. Stribeck who discovered it. As shown, friction may be divided into four regions depending on the origin of the friction. Friction occurs between two surfaces in contact. In mechanical systems, they are usually separated by some form of lubrication.

The first of the so called *lubrication regimes* is the *sticking regime*. Here the velocity between the surfaces is zero. The friction force in this regime is called static friction or *stiction*.

When the motion starts, the *boundary lubrication regime* is entered. In this, the friction is due to the oxide layers on the surfaces. Since they have

[2]See for example pp. 92-96 in Sears *et al.* (1987).

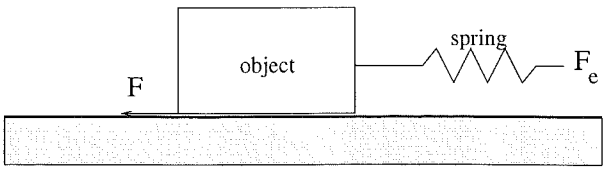

Figure 5 Stick-slip motion. The spring is pulled with increasing force until the box starts to move. After a sudden jerk, the box sticks again.

lower friction than the actual surfaces, the friction force is now decreasing with velocity.

In the *mixed lubrication regime* the surfaces are more separated than in the former one. The reason is that more lubrication has been brought in between them. The minimum of the Stribeck curve is located in this regime. The phenomenon that the curve is decreasing in the boundary lubrication regime and in the mixed lubrication regime is called the *Stribeck effect.*

In the *full fluid lubrication regime* the surfaces are completely separated. The friction is now due to the lubricant only, the surfaces are "water skiing" on the lubricant. The friction force is determined by the viscosity of the lubricant. Since this is proportional to velocity, the Stribeck curve in this regime is a straight line.

The Stribeck curve is not static. Depending on how the velocity is varied, one gets slightly different curves. Increasing the velocity gives slightly larger friction than decreasing it.

The concept of *break-away force* is important. It is the force required to initiate motion, i.e., to overcome the static friction. Experimentally, the break-away force of an object may be estimated by connecting a Newton meter to it and then pull this with increasing force until the object starts to move. The force required to start motion is then the break-away force. Since the static friction usually is lower than the kinetic friction and since a Newton meter usually contains a spring, the object usually will move for a while and then come to rest again. This is called *stick-slip motion.* The experimental setup is shown in Figure 5.

The break-away force varies with the rate by which the external force is increased. For low force rates the break-away force is larger than for high rates.

3.2 A Classical Model

Two mathematical models for friction will now be introduced. The first one is simple but satisfactory for less demanding tasks. The second one is advanced and state-of-the-art. It captures the properties described above along with some more. The two models will later be used in the practical experiments on the inverted pendulum. Among other things, their parameters will be identified. Let us start with the simple model.

The easiest model of friction force one can make is to approximate it with a constant, i.e, make it independent of velocity. This is called *Coulomb friction* and is denoted by F_C. Since the static friction force is larger than the kinetic friction force it would be more accurate to separate these two. Static friction is often shortened to *stiction* and denoted by F_S. As shown in Figure 4, the friction force in the full fluid lubrication regime is almost linear. This leads to the concept of *viscous friction*, denoted F_v, in which the friction force is considered proportional to velocity. Pure viscous friction is rare. Instead it is

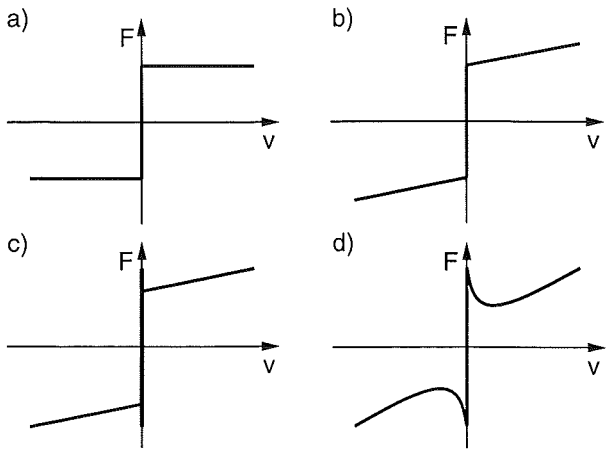

Figure 6 Classical friction models. In a), pure Coulomb friction is shown. In b), Coulomb friction is combined with viscous friction. In c), stiction is also in the game. d) shows a more realistic friction model, compare with Figure 4.

used in combination with Coulomb friction to form an affine relationship.

Figure 6 shows diagrams for the three different friction types. The relationships for both positive and negative velocities are shown. Since friction opposes motion, it has the same sign as the velocity.

The first of the two friction models to be used in this thesis is stiction with Coulomb friction. In mathematical terms, this is described by the following relationship:

$$F = \begin{cases} F_C \operatorname{sgn}(v) & \text{if } v \neq 0 \\ F_e & \text{if } v = 0 \text{ and } |F_e| < F_S \\ F_S \operatorname{sgn}(F_e) & \text{otherwise} \end{cases} \tag{17}$$

where F_e denotes the external force. The first line describes the Coulomb friction and the third the stiction level. The middle line says that if the object is at rest and the external force is less than the stiction, then the object does not move. The model has two inputs, the external force F_e and the velocity v, and one output, the friction force F. It is an example of a *static* friction model, i.e., it is stateless, the only things affecting the output are the present velocity and the external force.

The major advantage of (17) is its simplicity. It is easy to understand and it has few parameters, only two. It is also easy to implement, although a few problems arises, but they are common to most friction models. For a rough understanding and description of friction, (17) is therefore good.

The foremost advantage is also the foremost disadvantage. For more demanding tasks it is too simple. When studying kinetic friction at a detailed level it is not enough to approximate it by a constant. In that case static models are not enough.

3.3 The LuGre Model

In this section a more advanced friction model is introduced. It is naturally more complicated than the model in the previous subsection, but it will capture the properties mentioned in Section 3.1 along with other, more advanced.

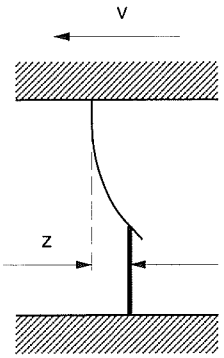

Figure 7 The contact interface between two surfaces may be considered as consisting of a single bristle. Its deflection is denoted by z.

The friction model is *dynamic*, i.e., it has a state z. Before giving the model, the state will be presented and motivated. Friction occurs when two surfaces are in contact. Since the surfaces are irregular, the contact takes place at a number of asperities. These may be modelled as elastic bristles. As a rough approximation all bristles may be replaced by a single one. Application of an external force causes the bristle to bend. Its deflection is denoted by z. See Figure 7.

We are now ready to give the model. It consists of a first-order differential equation in z, along with a formula for the output, the friction force F. The model has six parameters, among which F_S and F_C from the previous subsection are two.

$$\begin{cases} \dfrac{dz}{dt} = v - \dfrac{|v|}{g(v)}z \\ g(v) = \dfrac{1}{\sigma_0}(F_C + (F_S - F_C)e^{-(v/v_S)^2}) \\ F = \sigma_0 z + \sigma_1 \dfrac{dz}{dt} + F_v v \end{cases} \tag{18}$$

The model was first presented in Canudas de Wit *et al.* (1995). It is called the LuGre model since its pioneers came from Lund and Grenoble.

The friction force consists of three parts: stiffness, damping and viscous friction. The *coefficient of stiffness* is $\sigma_0 > 0$. It is constant and may be thought of as the stiffness of the bristle, i.e., how hard the surfaces are. The *coefficient of damping* $\sigma_1 > 0$ is also constant and affects the damping in the transition between sticking and sliding. The third term, the viscous friction, was explained in section 3.2.

The function $g(v)$ in (18) affects the shape and slope of the Stribeck curve in the boundary lubrication regime. The *Stribeck velocity* v_S affects the location of the minimum of the Stribeck curve, see Figure 4.

The model has many interesting mathematical properties. It is beyond the scope of this report to discuss them, but the eager reader may consult Olsson (1996). This also contains a more elaborate discussion of the parameters, comparisons with other models and simulation experiments.

There are a few extensions and variants of the model (18). The function $g(v)$ may, for example, be made asymmetrical or may be replaced by a function

other than an exponential one. F_S, F_C and F_v may also be made asymmetrical if the friction for positive velocities differs from that for negative ones. It is also possible to let σ_1 be a function of velocity. In Olsson (1996), the following equation is suggested:

$$\sigma_1(v) = \sigma_1 e^{-(v/v_d)^2}$$

If using the LuGre model, for example, to compensate for friction, an observer must be used. The reason is that the state z is not measureable. A simple observer is given below.

$$\begin{cases} \dfrac{d\hat{z}}{dt} = v - \dfrac{|v|}{g(v)}\hat{z} - ke \\ g(v) = \dfrac{1}{\sigma_0}(F_C + (F_S - F_C)e^{-(v/v_S)^2}) \\ \hat{F} = \sigma_0\hat{z} + \sigma_1\dfrac{d\hat{z}}{dt} + F_v v \end{cases} \tag{19}$$

Its structure is similar to a Kalman filter's, i.e., a correction term $-ke$ has been added to the system equation. The parameter k is the gain of the observer, e is an error, e.g., the control error. For mathematical properties and tests of this observer, see Chapter 5 in Olsson (1996).

3.4 Summary

An introduction to friction has been given and some of its properties have been presented, e.g., the Stribeck curve. There is an abundance of friction models. Two of these, one simple

$$F = \begin{cases} F_C \operatorname{sgn}(v) & \text{if } v \neq 0 \\ F_e & \text{if } v = 0 \text{ and } |F_e| < F_S \\ F_S \operatorname{sgn}(F_e) & \text{otherwise} \end{cases}$$

and one advanced

$$\begin{cases} \dfrac{dz}{dt} = v - \dfrac{|v|}{g(v)}z \\ g(v) = \dfrac{1}{\sigma_0}(F_C + (F_S - F_C)e^{-(v/v_S)^2}) \\ F = \sigma_0 z + \sigma_1\dfrac{dz}{dt} + F_v v \end{cases}$$

have been presented. A more thorough presentation is given in Olsson (1996).

4. Limit Cycles

The amplitude of a periodic solution to a linear system is dependent on the initial conditions. Different initial conditions give different amplitudes. Also, this kind of oscillation is not structurally stable since it is caused by solutions with purely imaginary eigenvalues. A *limit cycle* is a nonlinear oscillation whose size and shape is independent of the initial conditions, or more correctly, small variations in the initial conditions does does affect it.

4.1 Methods for Predicting Limit Cycles

It may often be desirable to predict whether a limit cycle will occur or not. And if it does, what its shape and character will be. Therefore, methods for predicting limit cycles have been developed.

A fairly simple such method is the Poincaré-Bendixson theorem. This states sufficient conditions for the existence of limit cycles for a given system. Unfortunately it only works in two dimensions, and has no correspondence in higher ones. Closely related is the Bendixson criterion. This states sufficient conditions for the non-existence of limit cycles.

The most famous, and probably most used, method for predicting limit cycles is the *describing function* method. A describing function may be said to be the nonlinear correspondence to the transfer function for linear systems. To use this method, the given system must be rewritten as consisting of two blocks, one linear and one nonlinear. Since a limit cycle is periodic it may be represented by a Fourier series. This is then truncated and only the first order term is kept. It is assumed that the input to the nonlinearity is a pure sinusoidal. The describing fuction is defined as the integral expression for the first order complex Fourier coefficient at the output of the nonlinearity, divided by some normalization constant. The describing function may be used to predict the existence of limit cycles, and if they occur, what their period and amplitude are most likely to be. The method is clearly approximative and it is known to have predicted wrong. Because of this approximativeness it is mostly used in applications, e.g., in automatic control.

None of the methods described above were used in this thesis. Instead simulation was used. By implementing the system and the nonlinearity in, for example, Simnon one gets, not only the period and amplitude of the limit cycle, but also its shape. By changing the parameters in the models one can easily see how the limit cycle changes. Simulation is not an exact method nor a mathematical one, but since a real system is not normally exactly known, it is, perhaps, the best method for use in this project.

The two theorems and the describing function method are described in detail in Khalil (1992). A study of limit cycles using simulation is done in Section 5 of this report.

4.2 Limit Cycles and Friction

Friction is a good example of a phenomenon which is closely connected with limit cycles. One example is *stick-slip motion.* It is associated with velocity control, and may occur in a system where the reference value is too small. A typical example of stick-slip motion is given in Section 3.1. The object will not get the desired velocity. Because of the friction it will alternate between slipping and sticking.

Another example is *hunting.* This may occur in position control where the controller has integral action. Because of the latter, the output will jump

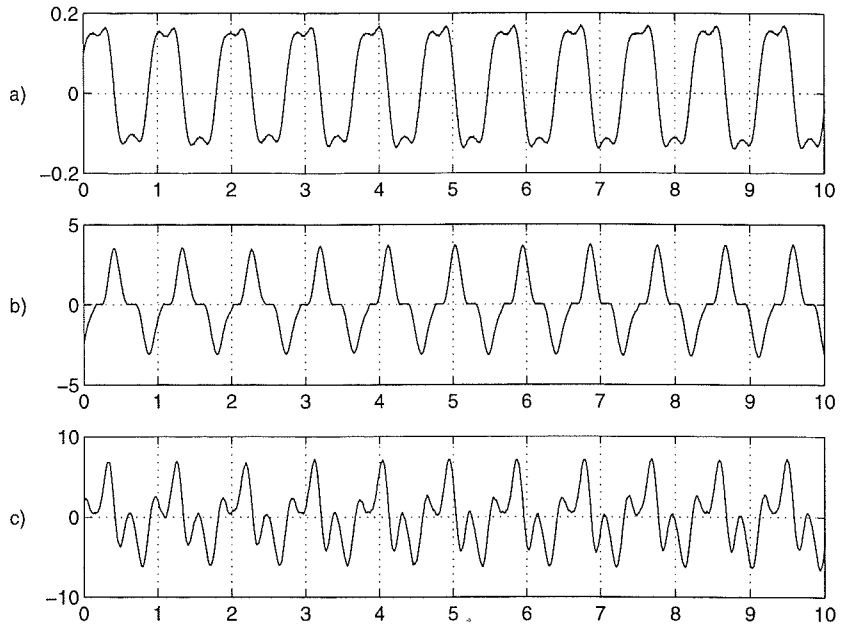

Figure 8 Typical limit cycles from the inverted pendulum. In a) the pendulum angle is shown, b) contains the velocity of the arm, and c) the control signal.

alternatively from one side of the reference value to the other without ever reaching it.

A third example of a system where limit cycles arise because of friction is the inverted pendulum. Since this is an unstable system with fast dynamics, the effect of friction is more severe than it would be on a corresponding stable system. When trying to balance the pendulum in the upright position, it starts to oscillate around it. The size and shape of this limit cycle varies with the controller parameters. Figure 8 contains a typical limit cycle. Three signals are shown, the pendulum angle, the arm velocity and the control signal. The real limit cycle was obtained using the linear state feedback loop described in Section 2. The fast arm control, (13) and (14), was used. Note that the arm is stuck for a short while at the turning points. This is most visible in the arm velocity.

In the next two sections, the relation between friction and limit cycles for the inverted pendulum are studied further. Also, more examples are given. The shape, amplitude and period of the limit cycles may be used to determine the size of the friction, and to identify friction models. This is also done.

4.3 Summary

Limit cycles are nonlinear oscillations. There are several methods to predict them, some of which have been presented briefly.

Because of friction, limit cycles often arise when trying to control mechanical systems. This is the case with the inverted pendulum. When trying to balance it, it oscillates. An example of this has been given.

5. Friction Identification Using Limit Cyles

There are many ways to estimate friction. And there are many ways to estimate the friction of the inverted pendulum. In Appendix E, simple direct methods are used. Stiction was, for example, estimated by sending out constant control signals of increasing magnitude until the arm started to move. There are two reasons why direct friction estimation is not a good method. The first is that it is rough. The second is that only simple static friction models can be identified. Estimation of the parameters in, for example, the LuGre model requires a more sophisticated method.

In this section, friction is estimated using limit cycles. As mentioned in the previous section, such arise when trying to balance the inverted pendulum. The period, amplitude and shape of the limit cycles depend on the friction. By comparing limit cycles from the real inverted pendulum with limit cycles obtained through simulation, the friction can be estimated and models identified.

For the simulations, the simulation language Simnon was used. The process model, the state feedback, the Kalman filter and the friction model were implemented in separate blocks. The algorithm used to solve the differential equations was Runge-Kutta-Fehlberg 4/5.

In Section 5.1, limit cycles from the real inverted pendulum are given and explained. Those are used to identify two friction models, the classical model (17) and the LuGre model (18). Section 5.2 is about the former and Section 5.3 is about the latter.

5.1 The Real Process

When trying to control the inverted pendulum using a simple, linear controller ones gets limit cycles. In this subsection, those are presented. The real-time controller described in Section 7 was used to register them. The state feedback and the Kalman filter described in Sections 2.2 and 2.3 acted as regulator. Two different parameter settings were used in the regulator, the fast control design, (13) and (14), and the slow control design, (15) and (16).

The Fast Control Design. A typical limit cycle from the inverted pendulum when the fast control design is used is shown in Figures 9–12. Eight signals are shown. The velocity of the pendulum is not measurable, and can thus not be plotted. In Table 1, amplitudes of the most important signals are collected, along with the period of the limit cycle.

Some remarks should be made regarding the shape of the limit cycle. The top of the cycles of the measured pendulum angle consist of two peaks with a valley in between. The first peak is lower than the second. See Figure 9.

The arm is stuck for a short while at the turning points. This is most noticeable in the plots for the measured arm velocity, since this is zero for short periods. The cause of the sticking is of course the stiction. The valleys in the measured pendulum angle are caused by the sticking, they coincide with the periods of zero arm velocity.

In Appendix E, one of the conclusions is that the friction is asymmetric and depends on the sign of the velocity of the arm. If this is the case, the limit cycle should be asymmetric. It is not. One may therefore deduct that the friction magnitude is not strongly dependent on the sign of the velocity.

In the Kalman filters friction was not considered. Therefore, the periods of zero velocity do not have any correspondence neither in the estimated arm

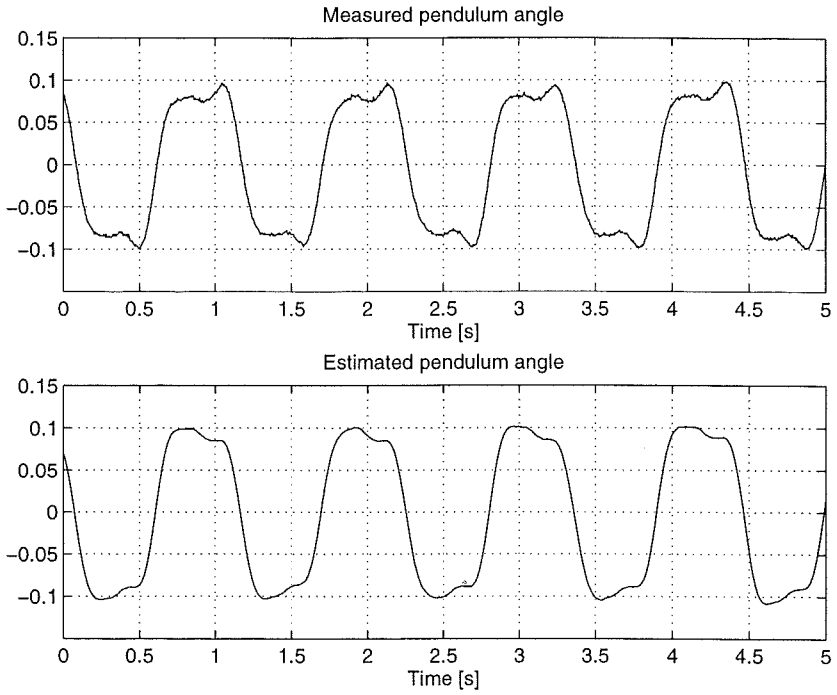

Figure 9 Limit cycles for the fast control design. Measured and estimated pendulum angle.

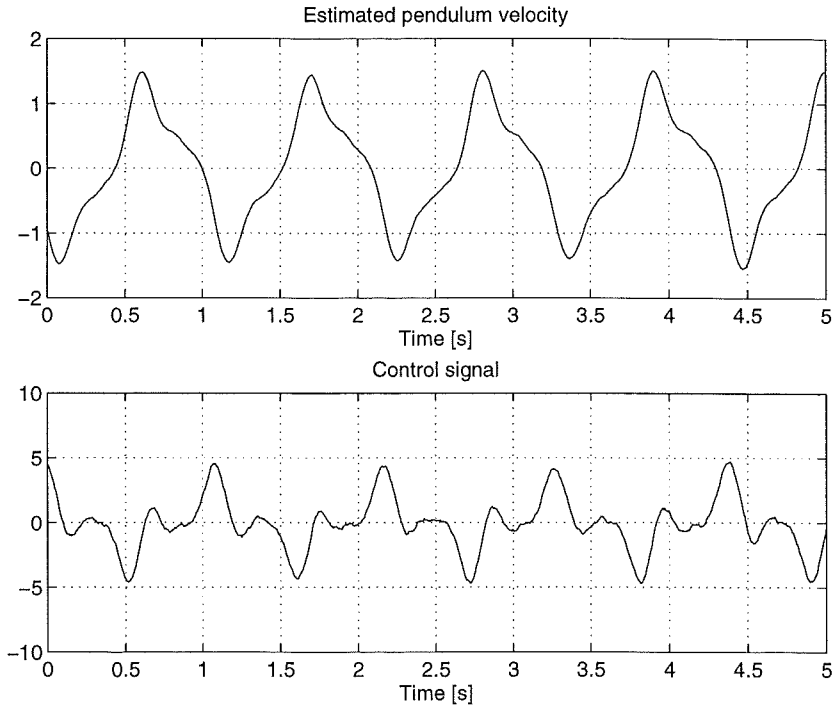

Figure 10 Limit cycles for the fast control design. Estimated pendulum velocity and control signal.

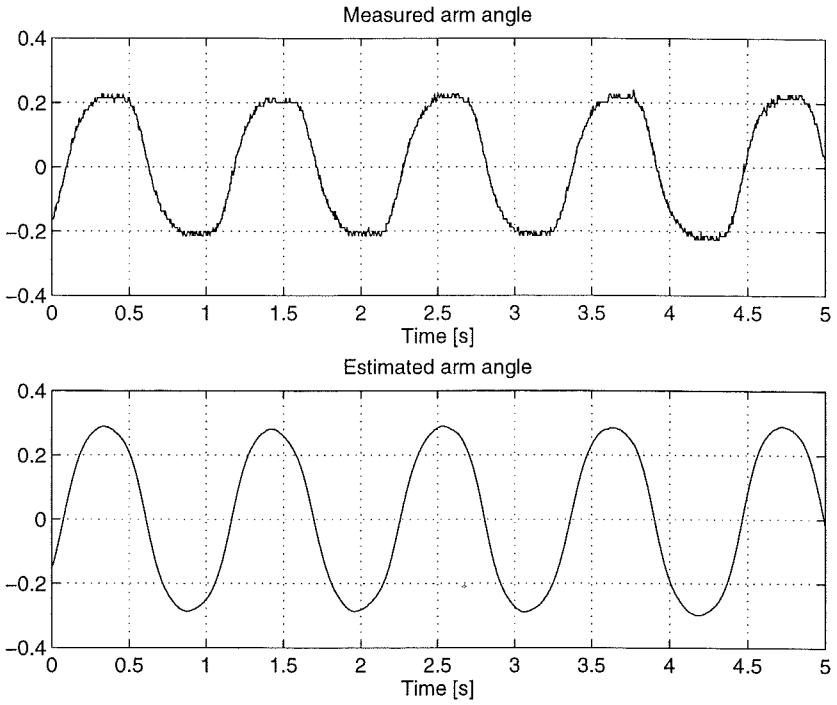

Figure 11 Limit cycles for the fast control design. Measured and estimated arm angle.

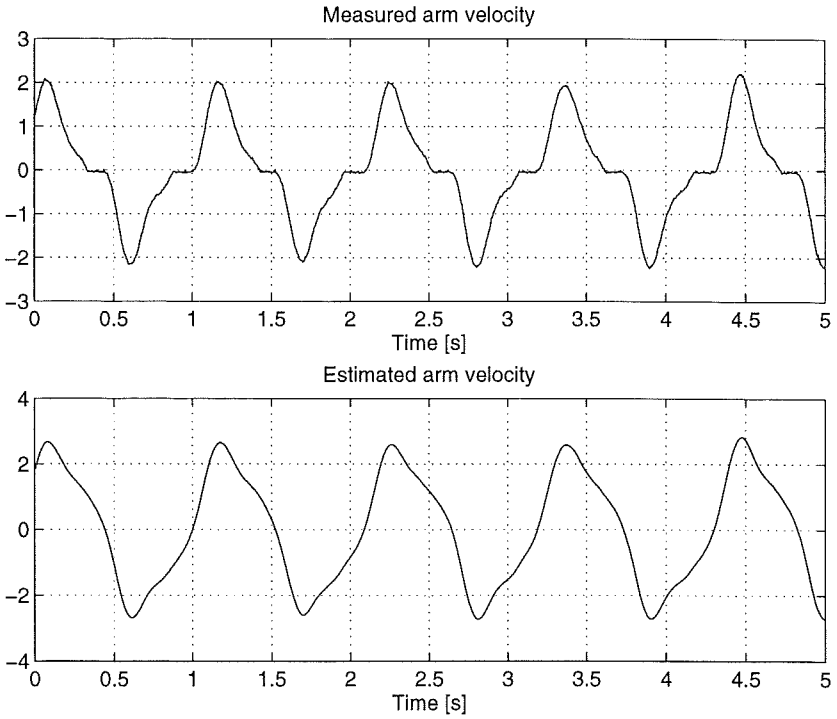

Figure 12 Limit cycles for the fast control design. Measured and estimated arm velocity.

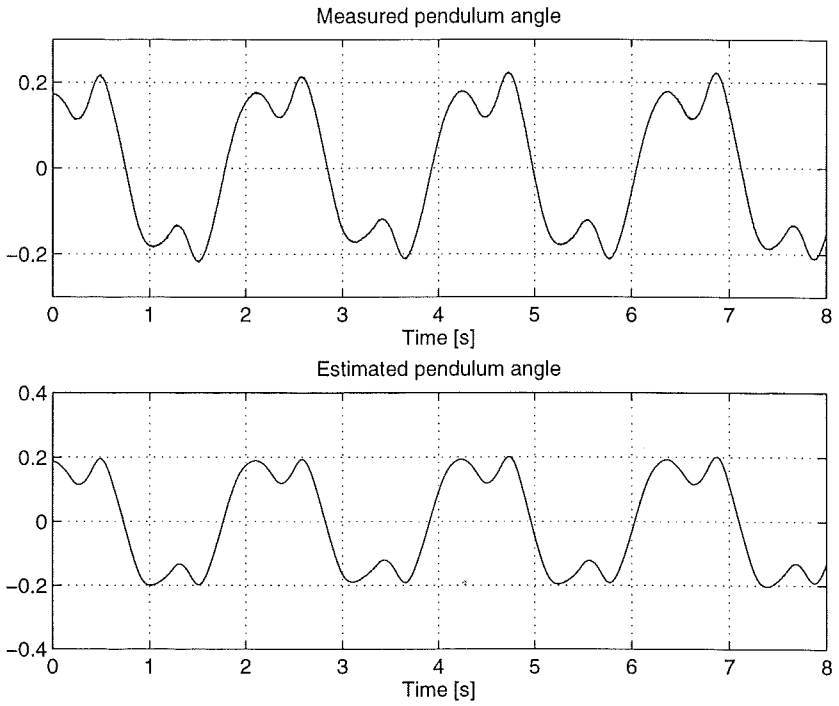

Figure 13 Limit cycles for the slow control design. Measured and estimated pendulum angle.

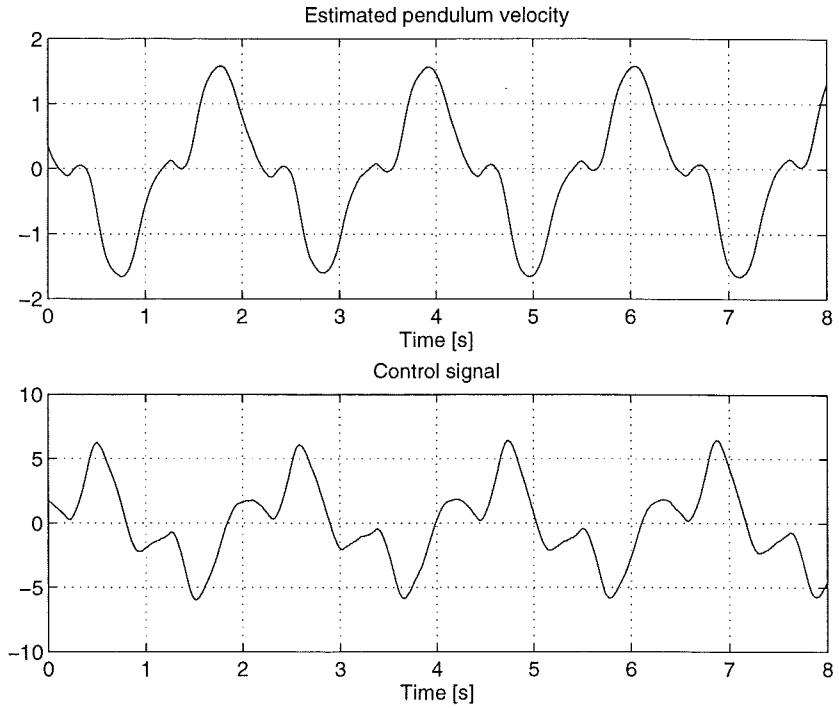

Figure 14 Limit cycles for the slow control design. Estimated pendulum velocity and control signal.

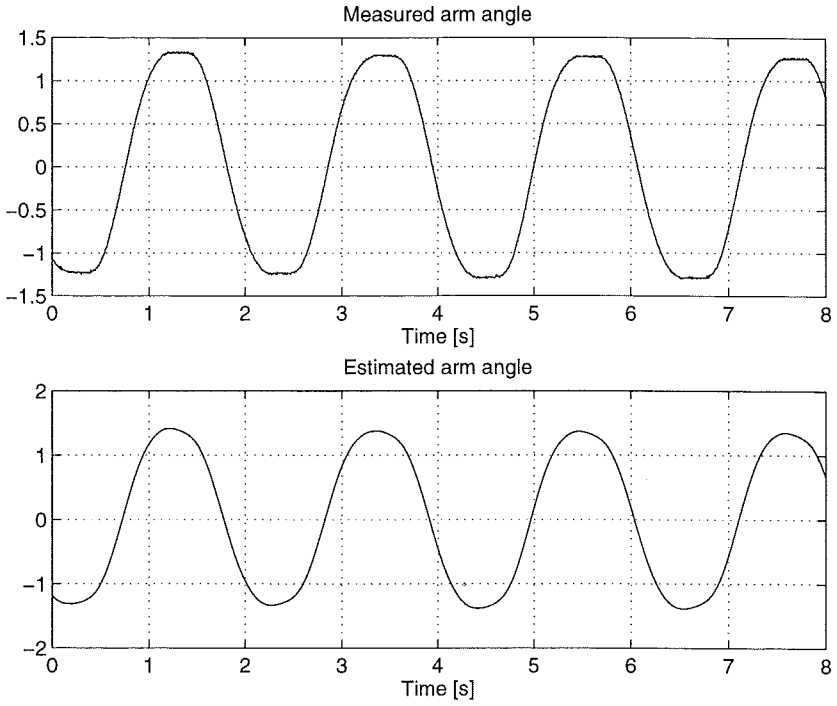

Figure 15 Limit cycles for the slow control design. Measured and estimated arm angle.

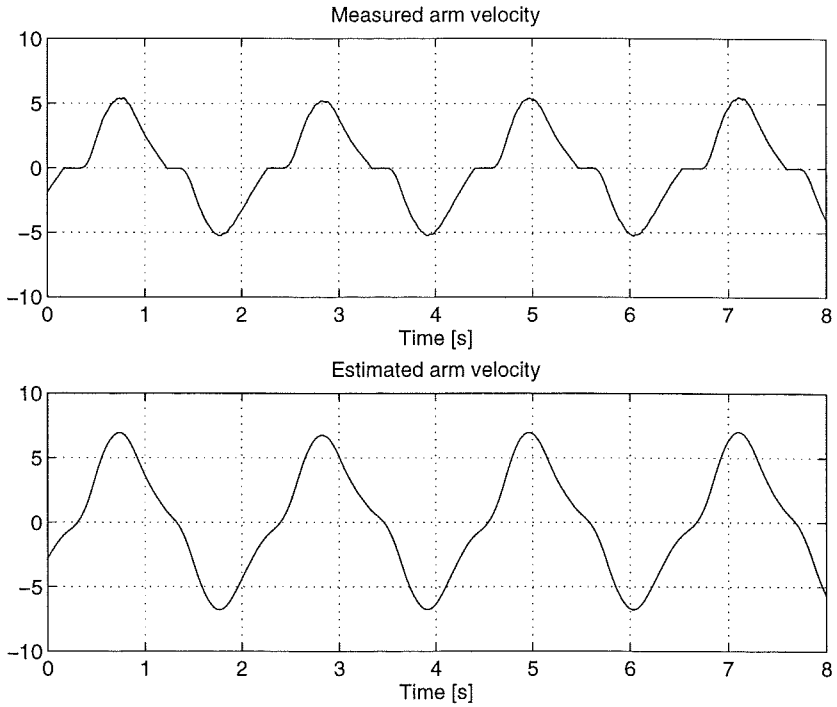

Figure 16 Limit cycles for the slow control design. Measured and estimated arm velocity.

angle nor in the estimated arm velocity.

The Slow Control Design. Figures 13–16 contain a typical limit cycle for the case of the slow control design. Table 1 contain some data for it.

Comparing with the limit cycle from the fast control design in Figures 9–12 one finds some similarities. The top of the cycles for the measured pendulum angle has the same shape in both control cases. However, the valley is more distinct in the present case. With two exceptions, the remaining signals are also similar to those in the fast case. The exceptions are the estimated pendulum angle and the estimated pendulum velocity. The former appears to be closer to its measured counterpart than in the fast case. This is explained by the fact that the limit cycle in the present case is slower than in the fast case.

The foremost differences between the two limit cycles are the period and the amplitudes. See Table 1. In the slow design, the period is 2.1 s, and the amplitude, i.e., from turning point to turning point, of the arm cycle is 145°, almost half a lap. In the fast design, the oscillations are faster and has a smaller arm cycle. The period here is 1.1 s, and the width is 23°.

	peak1	peak2	valley	T	max(u)	max($\dot{\Omega}$)
fast	0.080	0.095	0.074	1.1	4.4	2.0
slow	0.18	0.22	0.15	2.1	6.4	5.2

Table 1 Data for the real-time limit cycles. The heights of the two peaks of the measured pendulum angle are denoted by peak1 and peak2, and valley is the height of the valley. T is the period. max(u) and max($\dot{\Omega}$) are the maximum amplitudes of the control signal and the measured arm velocity. All parameters have SI units.

5.2 The Classical Model

The classical model (17) has only two parameters, the stiction F_S and the Coulomb friction F_C. Approximate values for them are given in Appendix E. For convenience, they are reproduced here.

$$\begin{cases} F_S = 2.3 \\ F_C = 1.5 \end{cases} \tag{20}$$

These estimates are used as initial values and as guidelines in the identification in this section.

The classical model is discontinuous, the friction force for zero velocity is larger than that during motion. When trying to simulate the model, problems arise because of this, since simulation is not exact. There are many possible solutions, the one used here is to define the interval $\dot{\Omega} \in [-0.001, 0.001]$ as being zero velocity.

Comparison of Limit Cycles. Comparison of limit cycles is the method used for the identification. It may be described as follows. Limit cycles from the real process are compared with limit cycles obtained through simulation. The friction parameters, F_S and F_C in this case, are varied systematically until the desired resemblance is obtained. Period and amplitudes are the most important factors, but the shape, for example of the measured pendulum angle, should also be considered.

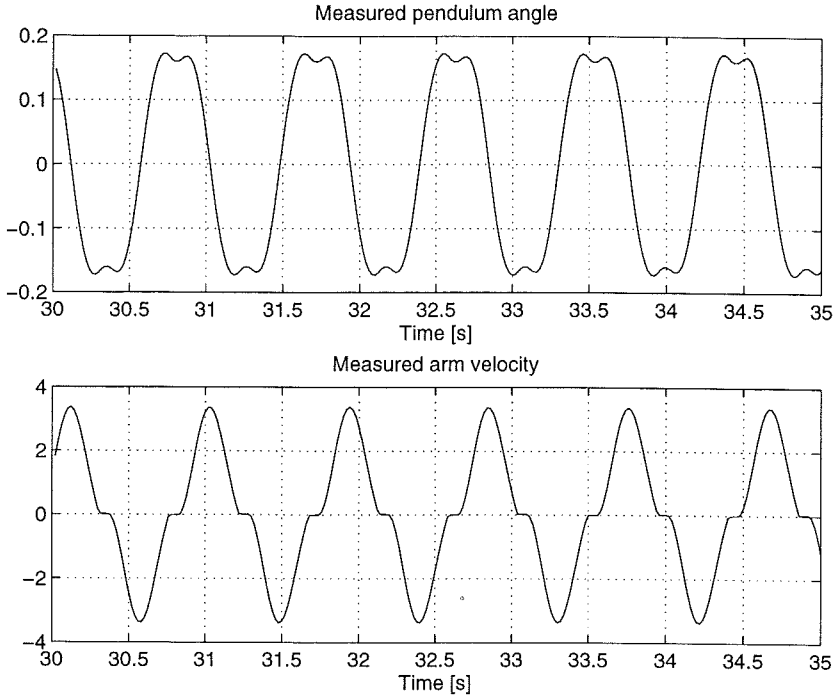

Figure 17 Simulated limit cycles for the fast control design. Measured pendulum angle and measured arm velocity. Compare with Figures 9 and 12.

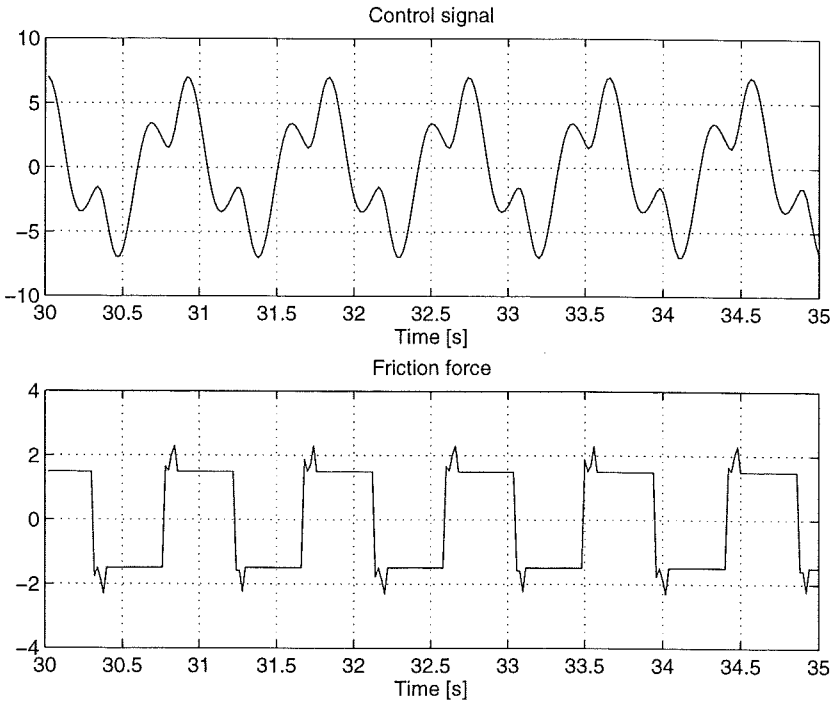

Figure 18 Simulated limit cycles for the fast control design. Control signal and friction force. Compare with Figure 10.

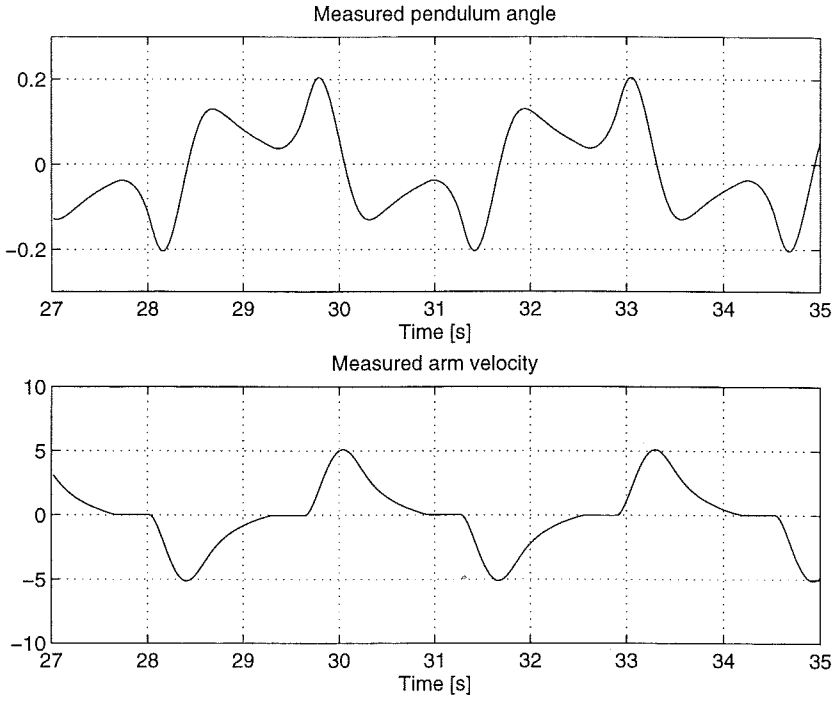

Figure 19 Simulated limit cycles for the slow control design. Measured pendulum angle and measured arm velocity. Compare with Figures 13 and 16.

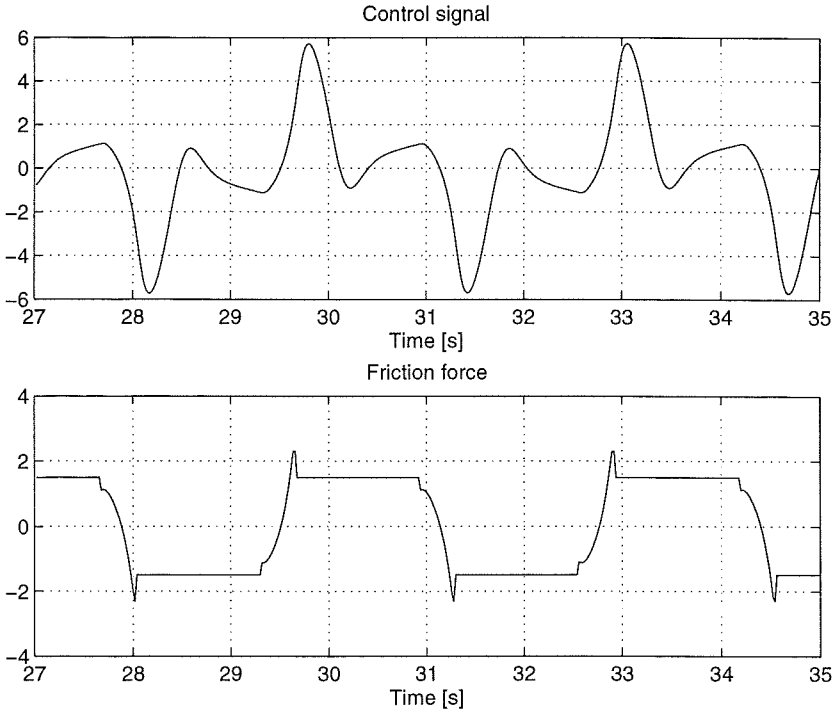

Figure 20 Simulated limit cycles for the slow control design. Control signal and friction force. Compare with Figure 14.

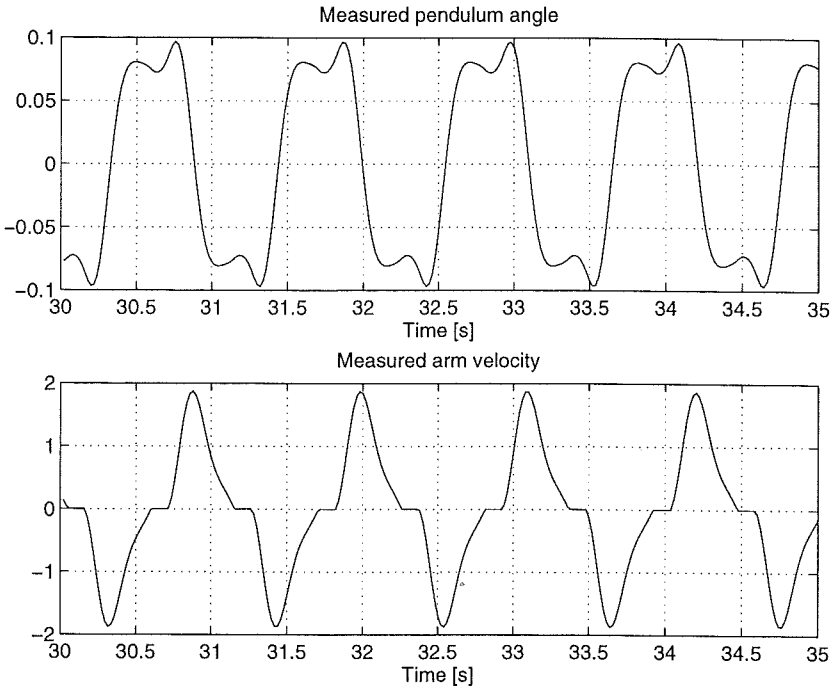

Figure 21 Simulated limit cycles for the fast control design when $\omega_0 = 7.5$, $F_S = 2.3$ and $F_C = 1.3$. Measured pendulum angle and measured arm velocity. Compare with Figures 9 and 12.

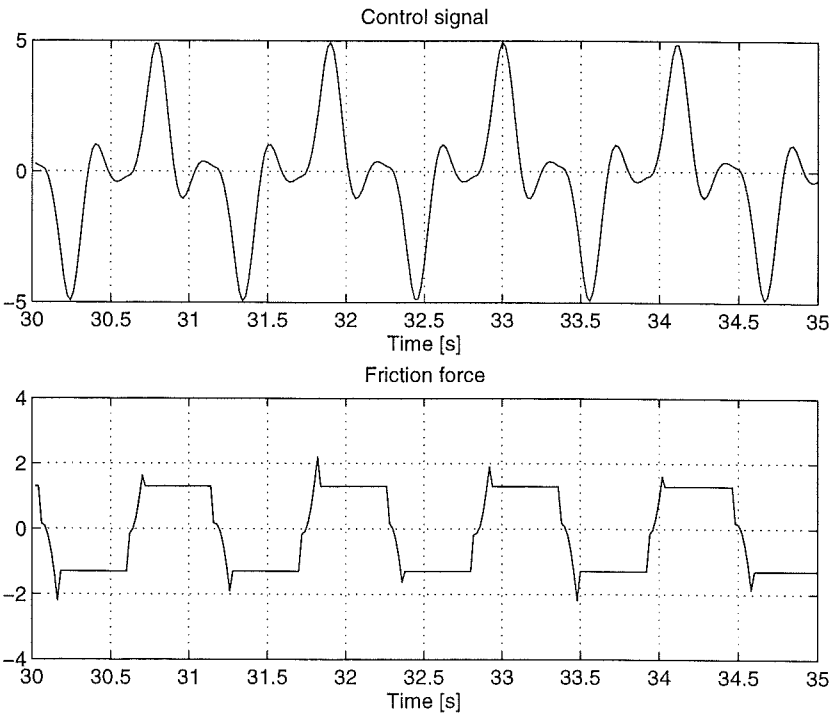

Figure 22 Simulated limit cycles for the fast control design when $\omega_0 = 7.5$, $F_S = 2.3$ and $F_C = 1.3$. Control signal and friction force. Compare with Figure 10.

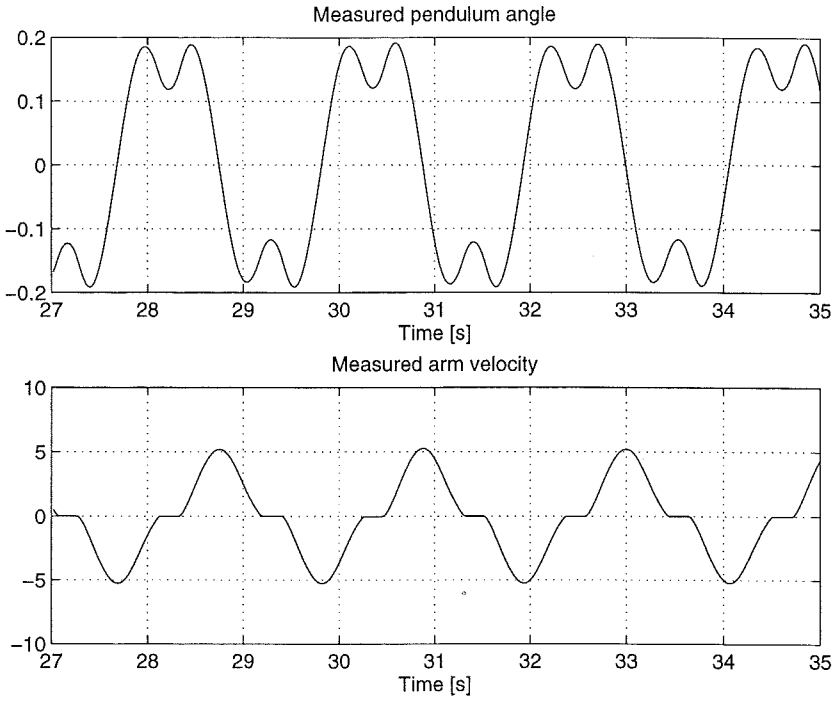

Figure 23 Simulated limit cycles for the slow control design when $\omega_0 = 6.1$, $F_S = 2.3$ and $F_C = 1.3$. Measured pendulum angle and measured arm velocity. Compare with Figures 13 and 16.

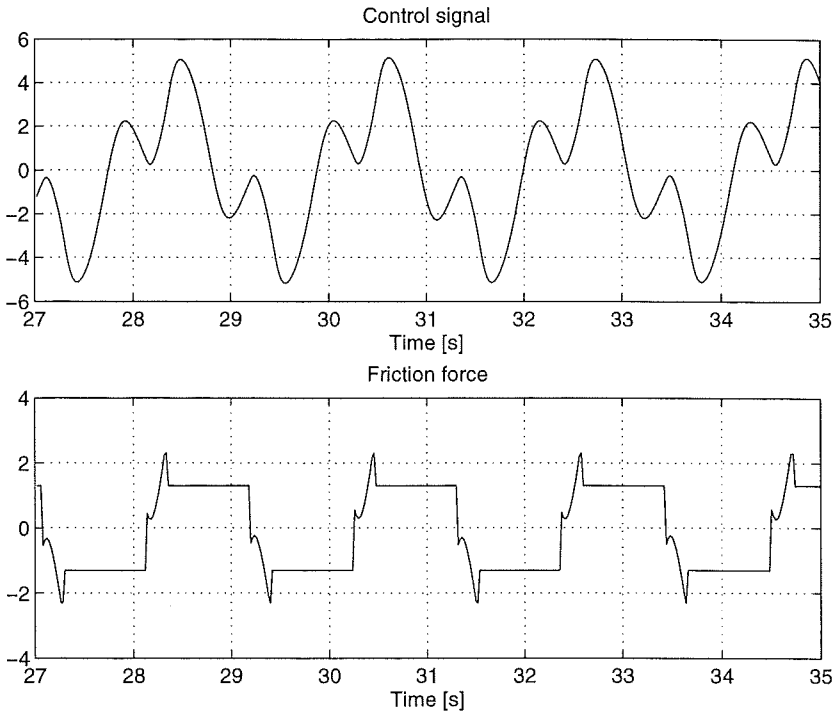

Figure 24 Simulated limit cycles for the slow control design when $\omega_0 = 6.1$, $F_S = 2.3$ and $F_C = 1.3$. Control signal and friction force. Compare with Figure 14.

F_C	peak1	peak2	valley	T	max(u)	max($\dot{\Omega}$)
1.1	0.143	0.142	0.135	0.888	6.0	2.70
1.3	0.157	0.154	0.146	0.901	6.5	3.05
1.5	0.172	0.168	0.159	0.911	7.0	3.35
1.7	0.187	0.182	0.172	0.916	7.6	3.70
1.9	0.199	0.192	0.182	0.921	8.2	4.00

Table 2 Variation of F_C in the case of the fast control design. The denotations are explained in Table 1. $F_S = 2.3$ was used as stiction.

F_S	peak1	peak2	valley	T	max(u)	max($\dot{\Omega}$)
1.9	0.169	0.164	0.157	0.920	6.7	3.23
2.1	0.171	0.165	0.157	0.916	6.8	3.31
2.3	0.173	0.167	0.159	0.910	7.0	3.35
2.5	0.176	0.172	0.164	0.900	7.3	3.45
2.7	0.178	0.174	0.165	0.897	7.5	3.50

Table 3 Variation of F_S in the case of the fast control design. The denotations are explained in Table 1. $F_C = 1.5$ was used as Coulomb friction.

Theoretically, this method should work. Practically, it does not. It is difficult to get good results when applied to the inverted pendulum. One reason is that the inverted pendulum is an unstable system with fast dynamics. Such a system is more sensitive to changes in the process parameters than a corresponding stable system. If accurate results are required, the process must be accurately known. Results from simulations are given below. They could not be used to find optimal parameters.

Simulation. Figures 17–20 shows simulated limit cycles. The first two figures contain cycles for the fast design, the last two figures contain cycles for the slow design. Because of lack of space, neither the estimated states nor the measured arm angle are included in the figures. Since the friction force is generated during the simulation, a plot of this is included. The period of the fast design is $T = 0.91$ s, and the period of the slow design is $T = 3.3$ s. Compare with Figures 9–16 in the previous subsection. In the case of the fast design, the period is smaller and the amplitudes are larger than those of the real process. The reverse is true for the slow design.

Variation of F_S and F_C. In the simulation described above, the friction parameters used are those determined by the rough methods in Appendix E. It was now tested if varying them would improve the correspondence. The fast arm control was considered first. In turn, F_S and F_C were varied, and for each setting the period and the peak amplitudes of the limit cycles were noted. The results are found in Tables 2 and 3. In order to get stiction, the interval of zero velocity had to be increased to $\dot{\Omega} \in [-0.03, 0.03]$.

Decreasing F_C while holding F_S constant at 2.3 results in lower maximum values and slightly smaller period. Increasing F_C yields the opposite. Decreasing F_S while holding F_C constant at 1.5 also reduces the amplitudes of the

F_C	peak1	peak2	valley	T	max(u)	max($\dot{\Omega}$)
1.1	0.096	0.154	0.028	3.17	4.3	3.6
1.3	0.109	0.174	0.032	3.26	4.8	4.2
1.5	0.125	0.194	0.036	3.32	5.4	5.0
1.7	0.141	0.217	0.038	3.38	6.0	5.8
1.9	0.162	0.241	0.042	3.39	6.9	6.7

Table 4 Variation of F_C in the case of the slow control design. The denotations are explained in Table 1. $F_S = 2.3$ was used as stiction.

F_S	peak1	peak2	valley	T	max(u)	max($\dot{\Omega}$)
1.9	0.122	0.189	0.036	3.32	5.2	4.9
2.1	0.124	0.191	0.036	3.33	5.2	4.9
2.3	0.125	0.194	0.036	3.32	5.4	5.0
2.5	0.126	0.198	0.036	3.30	5.5	5.0
2.7	0.128	0.198	0.035	3.31	5.6	5.0

Table 5 Variation of F_S in the case of the slow control design. The denotations are explained in Table 1. $F_C = 1.5$ was used as Coulomb friction.

limit cycles but increases the period. Variation of F_S affects the limit cycles less than variation of F_C. The experiment was repeated for the slow design, resulting in Tables 4 and 5. The behavior of the limit cycles is the same as for the fast design. The conclusion is that limit cycles resembling those from the real process cannot be obtained by varying the friction parameters, at least not within reasonable limits.

Explanations and Improvements. One may now ask oneself what to do in order to get the desired similarity. There are two possible answers to this question. The first is that the friction model may be too simple. If this is the case is tested in the next subsection, where the more advanced LuGre model is simulated. The second answer is that the model parameters and the conversion factors are not known exactly. The damping is almost negligible and, thus, does not affect the limit cycles to any extent. The length of the arm is very well known. The conversion factors for the pendulum angle, the arm angle and the arm velocity are also well measured. This leaves two parameters, the scaling factor for the control signal k_u and the natural frequency ω_0. When k_u is varied, the amplitude of the limit cycles are changed but not the period. The desired resemblance could therefore not be obtained.

Strangely enough, almost perfect resemblance is achieved in the case of the fast design by changing ω_0 in the process model from 6.8 to 7.5. The result is shown in Figures 21 and 22. Compare with Figures 9–12, the limit cycles from the real process. In the Kalman filter, ω_0 is kept at 6.8. I have not been able to explain why changing ω_0 gives this resemblance. Setting $\omega_0 = 7.5$ in the Kalman filter as well, gives limit cycles similar to those in the case when $\omega_0 = 6.8$, i.e., having the same ω_0 in the process model as in the Kalman filter gives bad resemblance. The best result that can be achieved in the case of the slow control is when ω_0 in the process model is decreased from 6.8 to 6.1. The

resulting limit cycles are shown in Figures 23 and 24. They are not as perfect as those for the fast design, but they are acceptable.

Summary. To summarize, simulating the system with the same ω_0 in the process model as in the Kalman filter gives poor results. Increasing ω_0 in the process model to 7.5 gives very good results for the fast design, but bad results for the slow design. Decreasing ω_0 to 6.1 and it is the other way around.

What the optimal friction parameters are will be left as an open question until Section 6. There, friction compensation is performed, and the friction parameters that reduce the limit cycles the most are determined.

5.3 The LuGre Model

Simulation of the classical model was not successful. Optimal friction parameters could not be determined by varying the friction parameters. Unfortunately, this holds for the LuGre model as well.

The LuGre model has seven parameters. Each of these was varied while the others were kept constant. As default parameters, the following values were used:

$$\begin{cases} F_S = 2.3 \\ F_C = 1.5 \\ F_v = 0.07 \\ \sigma_0 = 100 \\ \sigma_1 = 5 \\ v_S = 1 \\ k = 1 \end{cases} \tag{21}$$

Only the fast design was simulated. The results are found in Appendix F. As with the classical model, no parameters within reasonable limits made the limit cycles resemble those from the real process. When using the default values above, the simulated limit cycles resembles those in Figures 17 and 18 in the previous subsection. Setting $\omega_0 = 7.5$ gives limit cycles similar to those in Figures 21 and 22.

5.4 Summary

Simulation of the inverted pendulum with the two friction models was performed. It was not successful, limit cycles resembling those from the real process could not be obtained through simulation.

In Section 5.1, limit cycles from the real process were shown and explained. In Sections 5.2 and 5.3, simulation experiments using the two friction models were performed. The parameters of the models were varied in order to get limit cycles similar to those from the real process. This could not be achieved. The reason is that the process parameters and the conversion factors are not known accurately enough.

6. Model-Based Friction Compensation

There are many ways of reducing the effects of friction. The most common solution is to use some kind of lubrication. A better way is to use friction compensation. Using a friction model, an estimate of the friction force is calculated. This is then applied to the process with opposite sign towards the real friction force.

In this section, model-based friction compensation is tested on the inverted pendulum. As can be seen in Eq. (5), the friction force reduces the control signal. The friction force estimate should therefore be added to the control signal. Three friction models are used, the classical model (17), the LuGre model (18), and a pure Coulomb friction model. The real-time controller in Section 7 is used for the experiments. The same two control designs as in the previous section are used, i.e., the fast design (13) and (14), and the slow design (15) and (16).

The goal is to reduce the limit cycles as much as possible.

6.1 The Coulomb Friction Model

In theory, a model with pure Coulomb friction is a relay.

$$\hat{F} = F_C \operatorname{sgn}(\dot{\Omega})$$

In order to implement it for friction compensation it must be modified. Because of measurement noise, an arm velocity $\dot{\Omega}$ close to zero makes $\hat{F}$ toggle between $-F_C$ and F_C. In order to avoid this, hysteresis must be introduced. The limits are set to $\pm\varepsilon$. The model now has two parameters, F_C and ε. In Appendix E, the Coulomb friction is estimated to $F_C = 1.5$. Setting $\varepsilon = 0.05$ eliminates the toggling.

The results from the practical friction compensation were not good. When the parameters above are used, the limit cycles looks about the same regardless if friction compensation is on or off. Other values of F_C were tried as well, but the result was about the same. Setting $\varepsilon = 0$ makes the arm shake at the turning points. This results in shorter periods of stiction. But an oscillating control signal is bad for the motor, it wears it. Figures 25 and 26 contain a limit cycle along with the estimated friction force. The fast control design is used, and the friction parameters are $F_C = 1.5$ and $\varepsilon = 0.05$. Compare with Figures 9, 10 and 12. The slow design gives similar limit cycles.

The conclusion is that friction compensation using a pure Coulomb friction model is not fruitful in the case of the inverted pendulum. One reason is that the friction force is constant and only depends on the sign of the velocity.

6.2 The Classical Model

For two reasons, the classical model (17) is better than the model in the previous subsection. The first is that it has stiction, the second is that the size of the friction force depends on the control signal. It is therefore reasonable to expect better compensation with this model.

Two modifications must be made in order to use (17) in practice. The first is the same as for the previous model, hysteresis must be introduced. As above, the limits are set to $\pm\varepsilon$. The second modification concerns the discontinuity between the stiction and the Coulomb friction. This is eliminated by introducing an exponential decay of the friction force. After having done

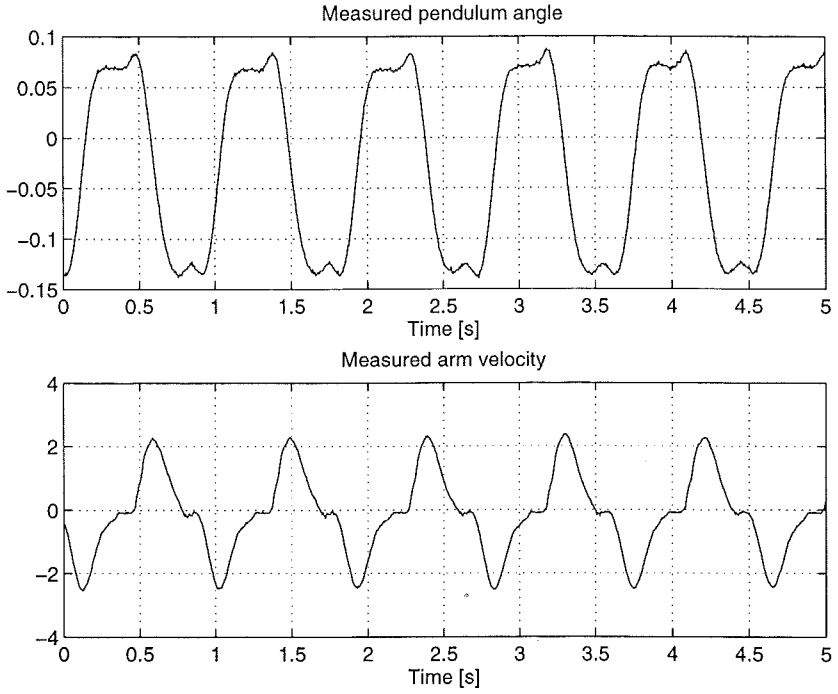

Figure 25 Limit cycle from the real process with friction compensation. The Coulomb model and the fast control design. $F_C = 1.5$ and $\epsilon = 0.05$. Measured pendulum angle and measured arm velocity. Compare with Figures 9 and 12.

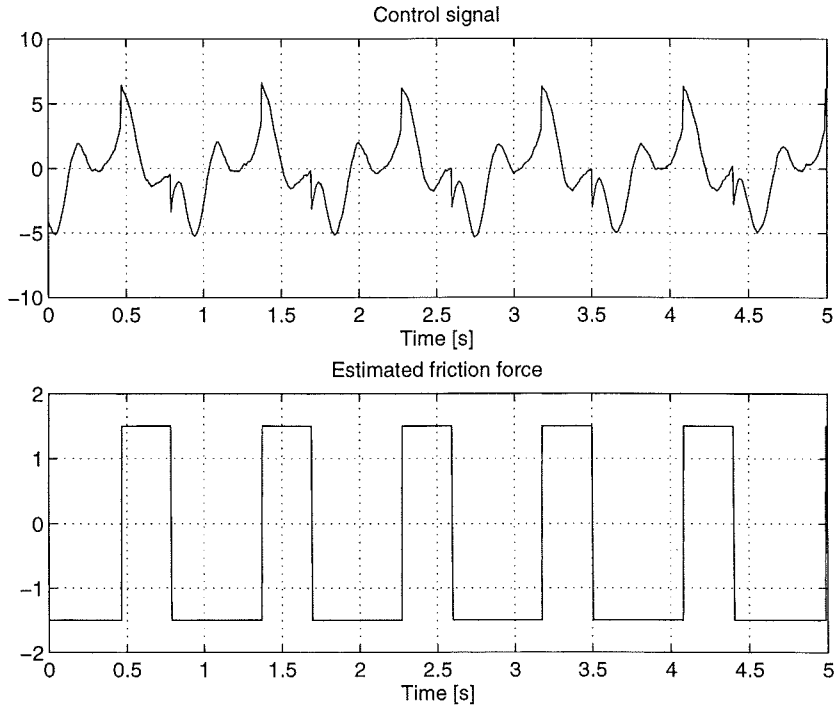

Figure 26 Limit cycle from the real process with friction compensation. The Coulomb model and the fast control design. $F_C = 1.5$ and $\epsilon = 0.05$. Control signal and estimated friction force. Compare with Figure 10.

these modifications, the implementation form of (17) becomes:

$$F = \begin{cases} u & \text{if } |\dot{\Omega}| < \varepsilon \\ \left(F_C + (F_S - F_C)e^{-(\dot{\Omega}/v_S)^2}\right) \operatorname{sgn}(\dot{\Omega}) & \text{otherwise} \end{cases}$$

As anticipated, friction compensation is better with the classical model. For the slow design, the following friction parameters reduce the limit cycles most:

$$\begin{cases} F_S = 2.3 \\ F_C = 1.55 \\ v_S = 0.5 \text{ or } 2 \\ \epsilon = 0.08 \end{cases}$$

The Coulomb friction F_C has to be increased slightly in order to get symmetric limit cycles. Two values of the slope v_S are optimal, depending on which type of limit cycle is preferred. The value $v_S = 2$ gives small but fast limit cycles. The smaller $v_S = 0.5$ gives slow but larger ones. In the latter case, the pendulum is better balanced. The former limit cycles resemble those in Figures 27 and 28, the latter those in Figures 29 and 30.

For the fast design, it is more difficult to reduce the limit cycles. The friction parameters above did reduce the limit cycles, but not as much as for the slow design. No better parameters than those above were found.

In both control cases, the arm oscillated slightly at the turning points.

6.3 The LuGre Model

The LuGre model is more flexible than the two previous models. It has more degrees of freedom, seven parameters. It is therefore easy to anticipate good compensation even for the fast design.

In the implementation, the LuGre model cannot be used as it is. Instead an observer must be used. The one used here is (19).

The friction parameters from Section 5.3 were used as starting point in the compensation experiments. One change was made, $F_C = 1.55$ was used since this gave symmetric limit cycles in the previous subsection. Some parameters affect the limit cycles more than others. In the quest for the optimal parameter setting, only three parameters were varied, σ_0, σ_1 and k.

If $\sigma_0 < 50$ the pendulum starts to shake, an undesirable behavior. Larger values increases the arm velocity. A σ_0 of about 400–500 makes the arm oscillate at the turning points. Smaller values of σ_1 than 5 make the arm more damped at the turning points. If $\sigma_1 = 10$ the motion gets jerky. The observer gain k is best placed between 5 and 10. Larger values make the arm shake, smaller make the limit cycles resemble those in the uncompensated case. The oscillatory behavior may be due to numerical problems in solving the differential equation of the LuGre model.

The friction parameters that best reduce the limit cycles for both control

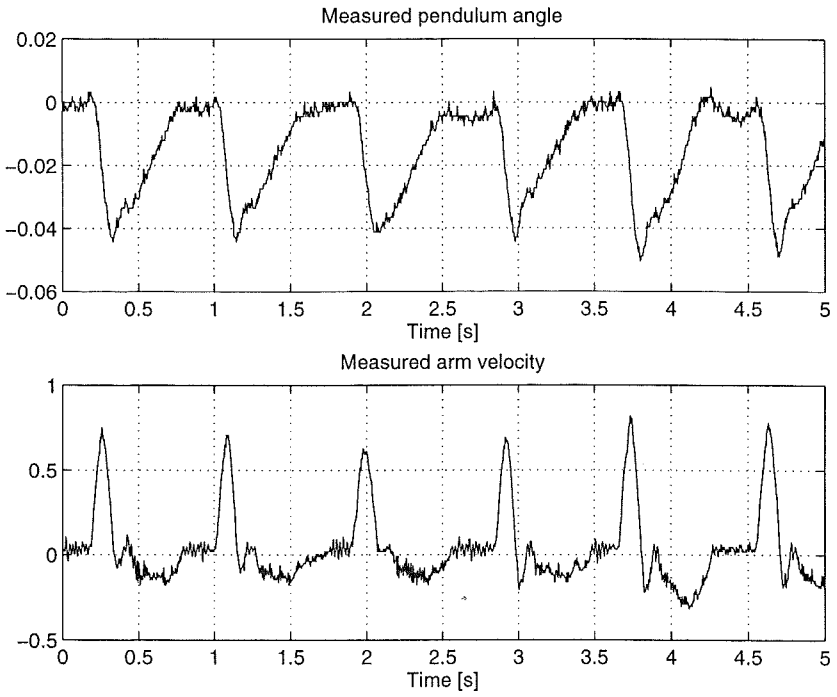

Figure 27 Limit cycles from the real process with friction compensation. The LuGre model and the fast control design. Measured pendulum angle and measured arm velocity. Compare with Figures 9 and 12.

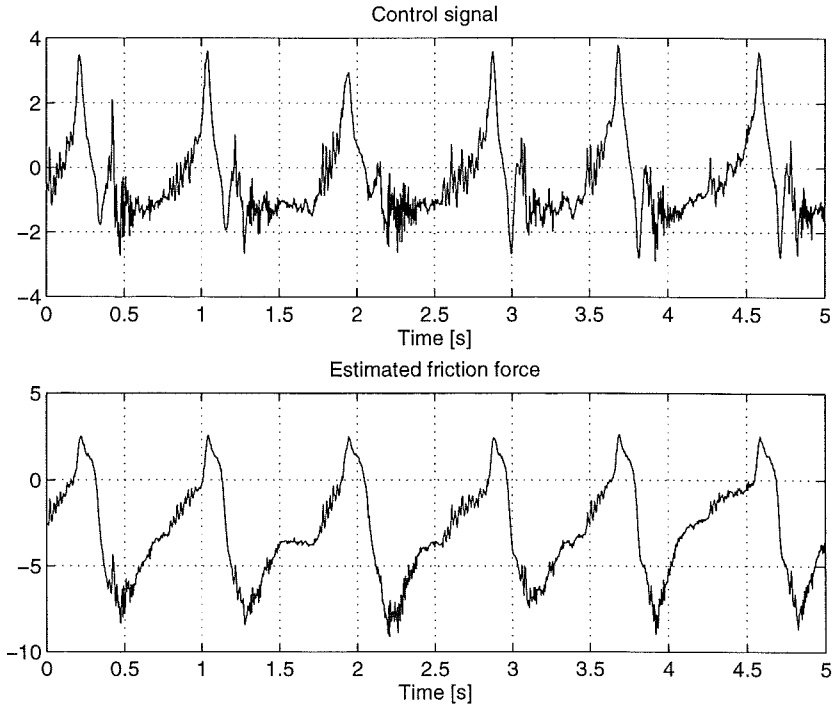

Figure 28 Limit cycles from the real process with friction compensation. The LuGre model and the fast control design. Control signal and estimated friction force. Compare with Figure 10.

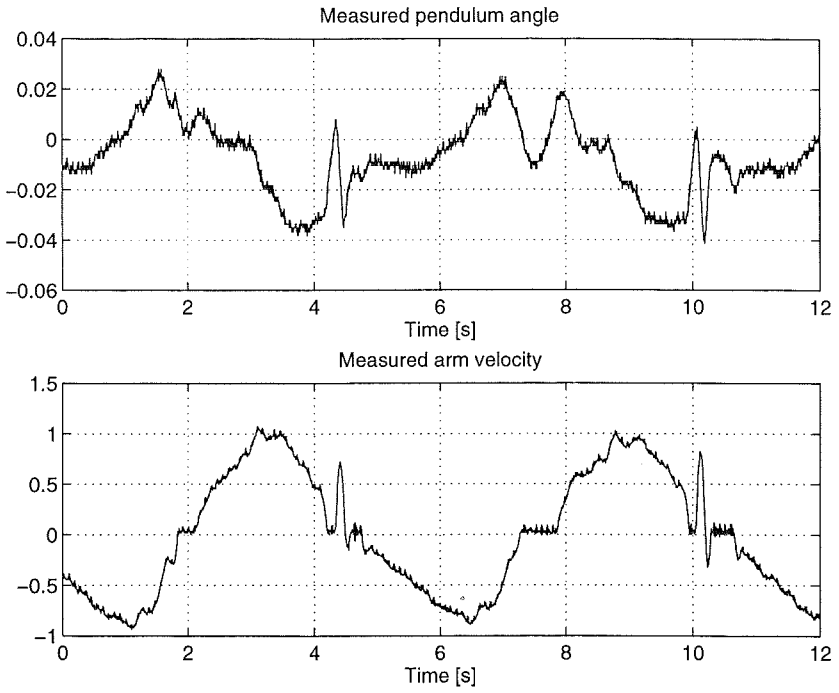

Figure 29 Limit cycles from the real process with friction compensation. The LuGre model and the slow control design. Measured pendulum angle and measured arm velocity. Compare with Figures 13 and 16.

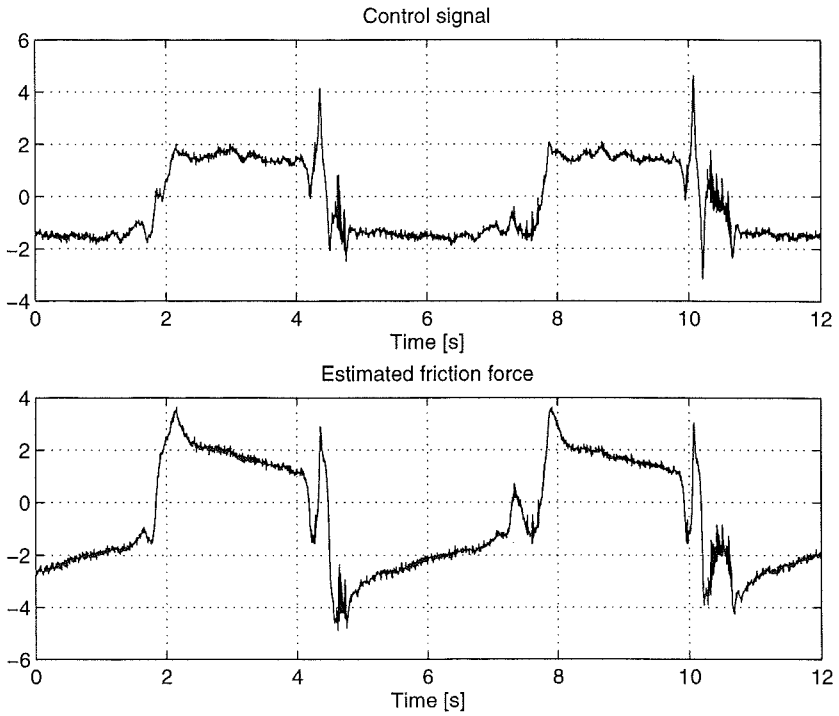

Figure 30 Limit cycles from the real process with friction compensation. The LuGre model and the slow control design. Control signal and estimated friction force. Compare with Figure 14.

designs are the following:

$$\begin{cases} F_S = 2.3 \\ F_C = 1.55 \\ F_v = 0.07 \\ \sigma_0 = 300 \\ \sigma_1 = 6 \\ v_S = 1 \\ k = 7 \end{cases}$$

Examples of resulting limit cycles are given in Figures 27–30. Note that they are asymmetrical. This has mainly two explanations, an asymmetrical friction force and bias in the measured pendulum angle.

For the fast design, the limit cycles are small and fast. The peak-to-peak value of the measured pendulum angle is about 0.04, compared to 0.2 in the uncompensated case. The period is about the same in both cases, a little smaller in the compensated case. For the slow design, the limit cycles are similar to those compensated with the classical model and $v_S = 0.5$, i.e., large and slow. Their behavior are unpredictable. In Figures 29 and 30, the peak-to-peak value of the measured pendulum angle is about 0.06 and the period is about 6 s. The corresponding values in the uncompensated case are 0.45 and 2.1.

Since the parameters given above best manage to reduce the limit cycles, it was tested what result they would give if simulated with. This was not successful, trying to simulate the LuGre model with them gave numerical problems.

6.4 Summary

Friction in the inverted pendulum is a nuisance and should be reduced. Lubrication is not enough, limit cycles arise anyway. Therefore, model-based friction compensation has been tried. Three models were used, one with pure Coulomb friction, the classical model and the LuGre model.

The result may be summarized as bad, better, best. The Coulomb model did hardly affect the limit cycles, they almost got larger. Better was the classical model. For the slow control design, improvement was clearly made, for the fast design, no. The LuGre model managed to reduce the limit cycles for both control designs.

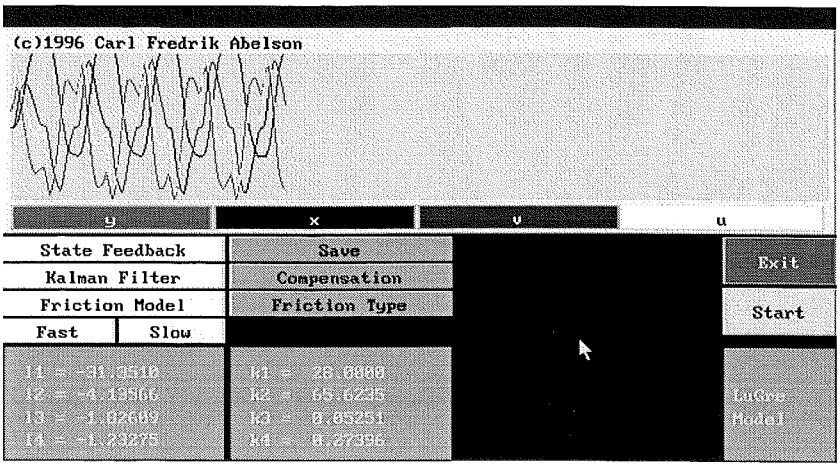

Figure 31 The real-time controller. Screen dump.

7. The Real-Time Controller

In order to perform experiments on the inverted pendulum, a real-time controller was written. The state feedback loop and the Kalman filter described in Section 2 were implemented. An MS-DOS computer was used as platform, and Modula-2 was used as programming language. The program is interactive, controller parameters may be changed on the screen.

Five cables must be connected between the inverted pendulum and the computer in order to transmit the measurements and the control signal. The table below describes how the cables should be connected.

Connection on IP	Port on computer
Armpos	AI 1
Hast	AI 2
PendelPos	AI 3
IN	AO 0
"Ground"	AGND on AO

7.1 User's Guide

The controller is interactive, parameters may be changed on the screen. The buttons for this are located in the lower part of the screen. In the upper part is a plot window. A screen dump is shown in Figure 31.

Start/Stop

The regulator is started by pressing the **Start** button on the right. Stopping it is done by the same button. No swing-up is implemented. Therefore, the pendulum must be balanced manually before starting the control.

Plot

The upper part of the screen consists of a plot window. When the regulator is active, signals are plotted. The signals plotted are the measured pendulum angle y, the measured arm position x, the measured arm velocity v, and the control signal u. By clicking on the buttons directly below the plot window, plotting of specific signals may be turned on and off.

Save Data

Use the **Save** button to save data. Collection of data is begun by pressing this key, and ended by pressing it a second time. Note that data are not stored to the disk directly. Instead this is done after the program has been exited. If having collected data, pressing the **Exit** button makes the program prompt for a filename. The prompt is called `out>`, and appears directly above the plot window. Input the filename with no extension! The extension `.dat` is added automatically.

The following ten signals are stored:

1. Measured pendulum angle θ
2. Estimated pendulum angle $\hat{\theta}$
3. Estimated velocity of pendulum $\hat{\dot{\theta}}$
4. Control signal u
5. Measured armposition Ω
6. Measured velocity of arm $\dot{\Omega}$
7. Estimated armposition $\hat{\Omega}$
8. Estimated velocity of arm $\hat{\dot{\Omega}}$
9. Estimated friction force F_{fr}
10. Estimated state z of the LuGre model

The data are placed in lines. They have ASCII-format and may therefore be loaded into Matlab.

Changing Controller Parameters

Parameters for the state feedback and for the Kalman filter may be changed. This is done using the two buttons **State Feedback** and **Kalman Filter** on the left. Click one of these, and a menu will appear. The current parameters are displayed. These are changed by pressing the value of choice, entering the new value, and pressing Return. Note that the new values are not set until the **Enter** button on the menu has been pressed. The controller parameters are explained in Section 2.

There are two shortcut keys, **Fast** and **Slow**. The first sets the controller parameters for the fast control design, (13) and (14), and the second is for the slow control design, (15) and (16).

Beneath the buttons described above, the current state feedback gains are displayed. To the right of them are the current Kalman filter gains.

Friction Compensation

Friction compensation is activated by pressing the button marked **Compensation** and deactivated by pressing it a second time. When the compensation is on, the text on the button is changed to **Compensating**.

The friction model used in the compensation is chosen by clicking on the button marked **Friction Type**. The current model is displayed in the text window in the bottom right corner of the screen. Three models are available, a model with Coulomb friction only, a classical model, and the LuGre model.

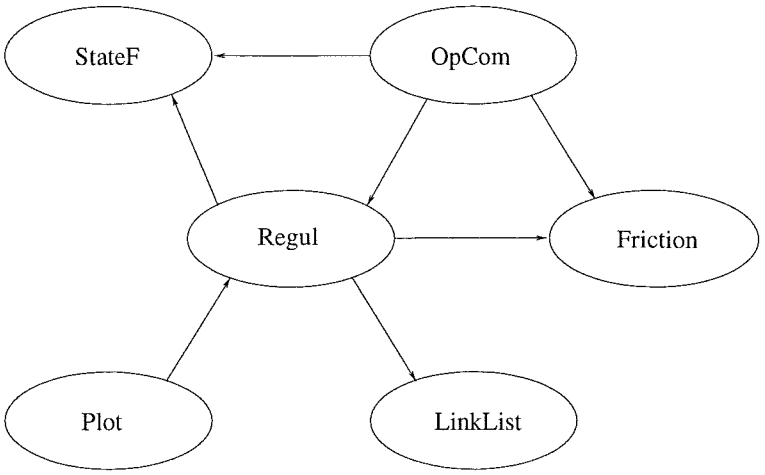

Figure 32 Dependency graph. By definition, the arrow point at the module being imported.

To change the parameters in the current friction model, use the button marked **Friction Model**. Press it, and a menu will appear. New parameters are entered in the same way as described in the section "Changing Controller Parameters" above. The parameters of the friction models are described in Section 3.

Exit

The program is exited by pressing the button marked **Exit**. Note that if data has been collected using the **Save** button, the program will prompt for a filename. See further Section "Save Data".

7.2 Module Structure

The program was written in Modula-2. In this language, a program is built on modules. A module consists of a collection of procedures and variables. In this subsection, the module structure of the controller is described. Figure 32 contains a dependency graph, showing the import dependencies between the modules.

Main The main module. Starts the processes, sets their priorities, and then waits for end. When the end signal comes from OpCom, the processes are terminated and the program is ended.

Regul The heart of the program. Contains the regulator process. Also procedure for sending measured data to the plot process.

OpCom Procedures for the operator communication. Buttons, menus and text windows.

Plot Controls the plotting of signals in the plot window. Contains the two plot processes.

StateF Support module for Regul. Contains the state feedback controller and the Kalman filter. Procedures for calculating the control signal, updating the states, getting and setting parameters, and updating the controller gains.

LinkList Using the "Save Data" button, data may be stored on disk. The collected data is not written directly, instead it is stored in a linked list until the program exits. This module contains the list plus procedures for handling it.

Friction Contains the friction models, and procedures for calculating the friction force.

7.3 Process Structure

Since the controller is a real-time system, it has processes. Their structure is described here. The program has four processes, two of which are located in the Plot module.

Regul The main control loop. Has the highest priority. Reads the measurable signals from the ADC, calculates the control signal, and sets it out on the DAC. Then updates the state of the Kalman filter. If data are to be stored, this is done. The process is periodic with period equal to the sampling period, $h = 0.005$ s.

OpCom The process for the operator communication is the mouse pointer. Each button has its own callback procedure. When the button is clicked, this is started. The mouse process is not periodic, it is event based. It has the second lowest priority.

Plot The plot module contains two processes. The first, Read, gets the measured data from Regul and puts it in a buffer. This process has the second highest priority and is periodic with period 0.1 s. The other process, Plot, collects the data from the buffer and plots it. This is non-periodic and has the lowest priority.

7.4 Process Communication

The communication between the processes is handled using monitors. Associated with each monitor is a collection of monitor procedures. In these, the shared variables are accessed.

Instead of each process having its own monitor, as would be the more natural solution, each module has its own monitor. Although a bit circumstancial, this solution works perfectly. In future versions of the program, however, this will be changed.

7.5 Summary

In this brief section, the real-time controller was described. It was written in order to perform experiments on the real inverted pendulum. A user's guide for the program was given. The internal structure of the program was described, its modules, processes and process communication.

8. Summary and Conclusions

Friction is a difficult phenomenon. There is no standard model that captures all of its properties. A vast number have been proposed, and which is the best depends on the application. There is also no universal way of estimating friction. This also depends on the application.

In this thesis, friction in an inverted pendulum has been studied. The friction has been modelled, identified and compensated for. For the modeling, two friction models were used. One simple, static and classical with stiction and Coulomb friction, and one advanced, dynamical and state-of-the-art, the LuGre model. Both of these are good in capturing the friction of a mechanical system like the inverted pendulum. They are introduced in Section 3.

Friction identification was performed using two methods. The first is simple. It regards friction from a mechanical point of view. This method is described in Appendix E. The second method is based on comparison of limit cycles. When trying to control the inverted pendulum using a simple linear controller one gets limit cycles because of friction. Limit cycles from the real process were compared with limit cycles obtained through simulation. Unfortunaretly, this method was not very successful. It requires a process model with accurately known parameters. An unstable process with fast dynamics, like the inverted pendulum, is very sensitive to changes in the process parameters. A small change in one parameter makes a great change in the shape of the limit cycles. The result from the simulations are given in Section 5.

Friction compensation was more successful. The limit cycles were reduced. It was not possible, however, to make the pendulum stand still. Best results were achieved with the LuGre model. A third friction model was introduced, pure Coulomb friction. This model is extermely simple and one of the most commonly used in practical friction compensation. It was not successful in the case of the inverted pendulum, however. Friction compensation is discussed in Section 6.

A nonlinear model of the inverted pendulum was derived, and its parameters were identified. This was required for doing the experiments described above. Linear state feedback was used as regulator, with Kalman filters for estimating the states of the process. The controller was implemented using a real-time computer.

Two major conclusions may be drawn from the experiments, one negative and one positive. Friction identification based on limit cycles is difficult and requires an accurately known process model. It was not possible to estimate better friction parameters than those determined using simple methods. The positive conclusion is that friction compensation is practically feasible, the limit cycles were indeed reduced.

Some aspects of friction in the inverted pendulum has been studied in this thesis. Since friction is a complex phenomenon, there are many more which could have been studied, but unfortunately time was the limit. Two possible extensions will be mentioned. The process parameters and the conversion factors should be estimated more accurately, so that friction identification using simulation of limit cycles could be performed better. Also, it would be interesting to test an adaptive friction estimator, since friction varies slightly with the operating conditions.

A possible non-friction extension is to implement a swingup for the pendulum. Control strategies other than linear state feedback could also be tried, e.g., fuzzy control.

A. Identification of the Inverted Pendulum

There are many ways to identify a process. One method is to use a pseudo random binary signal as input to the process, and then identify the collected data using Matlab's System Identification Toolbox. Unfortunately it is difficult to get good results with this method for the inverted pendulum. For a try, see Abelson and Christelius (1996). Instead, heuristic or direct methods have to be used.

The model (4) for the inverted pendulum has three parameters, the resonance frequency ω_0, the damping ζ and the length of the arm L_1. In section 2.1 values for these are given. In this appendix, the values will be motivated and the experiments used to determine them will be presented.

A.1 The Resonance Frequency ω_0

Linearizing Eq. (4) around the downward position $\theta = \pi$ yields a linear process model. Its characteristic polynomial may be written as

$$s^2 + 2\zeta\omega_0 s + \omega_0^2$$

This corresponds to a differential equation for θ.

$$\ddot{\theta} + 2\zeta\omega_0\dot{\theta} + \omega_0^2\theta = 0$$

The solution of this is

$$\theta(t) = Ae^{-\zeta\omega_0 t}\cos(\omega_d t + \phi) \tag{22}$$

where

$$\omega_d = \omega_0\sqrt{1-\zeta^2} \tag{23}$$

The constants A and ϕ may be determined by initial conditions.

The most accurate method of estimating the resonance frequency for a process is to determine its Bode plot. The resonance frequency is then the frequency at which the peak of the amplitude curve is located. Since the damping affects the position, it has to be taken into account. However, this method was not used. Instead a less accurate but simpler one was used. The arm of the inverted pendulum was held tight while the pendulum was manually set in motion. RT-Simnon, run in open loop, recorded the oscillations. The result is shown in Figure 33.

If the damping is small enough, $\omega_0 \approx \omega_d$. In this subsection this approximation is made. In the next subsection, the damping is estimated and, if necessary, ω_0 corrected. Not taking the damping in account, ω_0 may therefore be estimated using the following formula:

$$\omega_0 = \frac{2\pi}{T} \tag{24}$$

where T is the period of the oscillations. T will be estimated by measuring the average distances between the peaks marked in Figure 33. Since the oscillations are nonlinear, peaks whose amplitude is larger than, say, 0.15 rad will be considered unreliable. Because of friction in the pivot point, the last oscillations will not be used either. The location of the peaks are shown in the table below. They have been measured from the diagram using a ruler.

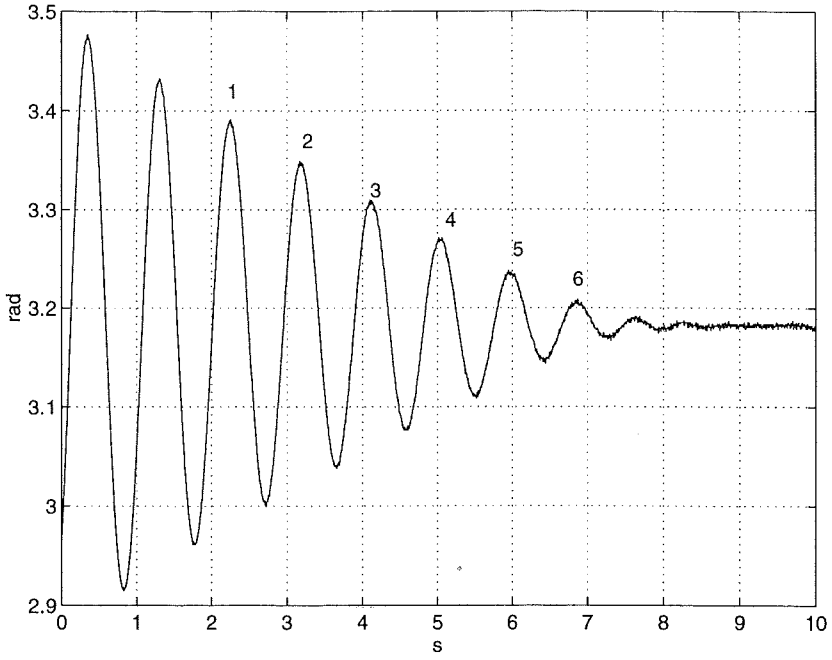

Figure 33 Damped oscillations. The digits mark the peaks used in the estimations.

peak	t	$\Delta t = t_i - t_{i-1}$
1	2.25	—
2	3.23	0.98
3	4.11	0.88
4	5.06	0.95
5	6.01	0.95
6	6.87	0.85

The average distance between the peaks is the average of the values in the Δt-column, and it is $T = 0.92$ s. Using Eq. (24) above, an estimate of ω_0 is

$$\omega_0 = \frac{2\pi}{0.92} = 6.83 \text{ rad/s}$$

Since damping affects this value, it will be corrected in the next subsection.

A.2 The Damping ζ

In Figure 33, one clearly sees that the oscillations are damped. In this subsection the size of this damping is estimated. If the oscillations obey Eq. (22), then the amplitudes of their peaks are approximately given by

$$\theta_{peak}(t) = Ae^{-\zeta\omega_0 t} \tag{25}$$

Since ω_0 is known, the peaks of the oscillations may be fitted to this equation. The same peaks as in the previous subsection are used. Their heights were calculated using a ruler. The result is shown in the table below.

peak	θ	$\theta - \theta_0$	t	$t - t_0$
1	3.39	0.21	2.25	0
2	3.35	0.17	3.23	0.98
3	3.31	0.13	4.11	1.86
4	3.27	0.09	5.06	2.81
5	3.24	0.06	6.01	3.76
6	3.21	0.03	6.87	4.62

The second column shows the absolute pendulum angles, as measured from Figure 33. In the third, these have been corrected so that the downward position, $\theta_0 = 3.18$ rad, corresponds to zero angle. It is the values in this column that will be fitted to the equation above.

The fourth column contains the time locations of the peaks. In the last column, the time scale has been corrected so that the first peak corresponds to $t = 0$. The height of the first peak was used as A. ζ was calculated for each of the other peaks by the following modification of Eq. (25):

$$\zeta = -\frac{1}{\omega_0 t} \ln(\frac{\theta}{A})$$

where θ and t are taken from the table and $\omega_0 = 6.83$ is the value estimated in the last subsection. The following dampings resulted:

peak	ζ
2	0.032
3	0.038
4	0.044
5	0.049
6	0.062

The damping estimates vary very much. One reason is friction in the pivot point. As the amplitude of the oscillation decreases, the effect of this friction increases. Therefore, the damping estimates for the higher peaks are the more reliable. Somewhat arbitrarily, the value $\zeta = 0.04$ was chosen as the final damping estimate. Because of the uncertainty, it is given with one digit only.

Because of the damping, the resonance frequency estimated in the previous subsection was ω_d, not ω_0. Since an estimate of the damping is now available, ω_0 will be calculated. Using Eq. (23) one gets

$$\omega_0 = \frac{\omega_d}{\sqrt{1-\zeta^2}} = \frac{6.83}{\sqrt{1-0.04^2}} = 6.84 \text{ rad/s}$$

The assumption that $\omega_0 \approx \omega_d$ therefore was valid. Because of the rough method used, only one decimal is used, yielding the estimate $\omega_0 = 6.8$ rad/s.

A.3 The Length of the Arm L_1

The length of the arm of the inverted pendulum was measured using a ruler. The distance from the axis of rotation at the center pillar to the pivot point is $L_1 = 0.21$ m.

A.4 Summary

Using simple methods, good estimates of the process parameters have been calculated. They were

$$\begin{cases} \omega_0 = 6.8 \text{ rad/s} \\ \zeta = 0.04 \\ L_1 = 0.21 \text{ m} \end{cases}$$

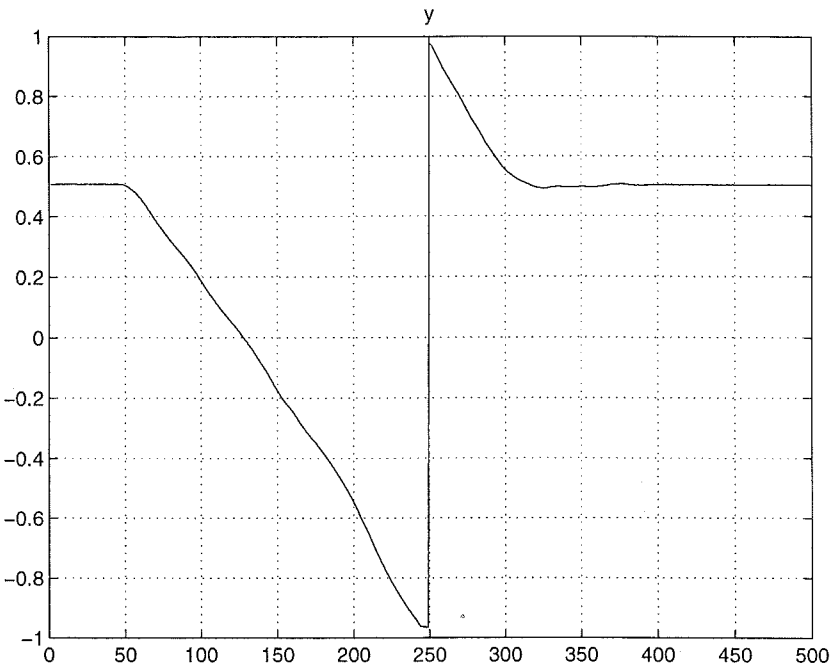

Figure 34 The angle of the pendulum. On the y-axis is the unscaled and biased angle read from the ADC, and on the x-axis is the number of data points.

B. Measuring the Conversion Factors

The signals received from the AD-converter (ADC) and the signal sent to the DA-converter (DAC) are scaled and biased and not in SI units. Since it is desirable to work with unbiased SI units inside the regulator, the signals must be converted to such. To do this, the scaling factors and the biases — conversion factors for short — must be known.

The inverted pendulum has three outputs: the angle and the velocity of the arm, and the angle of the pendulum. It has one input: the control signal. Below conversion factors for these will be presented along with the experiments used to determine them.

B.1 The Angle of the Pendulum

The scaling factor for the pendulum angle was determined by manually rotating the pendulum one lap, from downward to downward position. During the revolution, the angle of the pendulum was measured. The result is shown in Figure 34. As can be seen, the pendulum goes from about -1 to 1 in one lap. Since one lap in SI units corresponds to 2π radians, the scaling factor is approximately π. This is not entirely correct, the scaling factor is slightly less than π, but this value is used anyway.

Besides the fact that the measured and the real pendulum angle differs by a scaling factor, there is also a bias between them. When the pendulum is in its upright position, the ADC does not return the value zero. The measured zero is instead located around $\pi/2$ rad. The reason is that it is undesirable to have the leap from -1 to 1 in or near the upright or the downward position. Measuring the bias was simple. The pendulum was balanced manually in its upright position and the signal from the ADC was read. The value -0.503

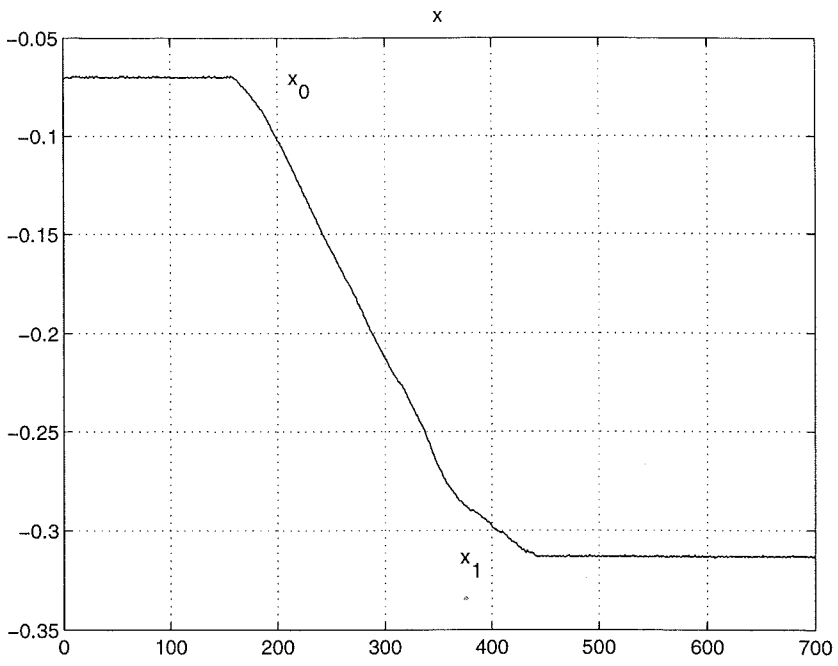

Figure 35 The angle of the arm. On the y-axis is the unscaled, measured angle, on the x-axis is the number of data points.

resulted.

To summarize, we have the following conversion formula between the measured pendulum angle y and the real pendulum angle θ. By definition $\theta = 0$ means a pendulum in its upright position.

$$\theta = \pi(y + 0.503) \quad y \in [-1, 1]$$

B.2 The Angle of the Arm

An ADC has a limited range. For example, the ADCs on the inverted pendulum are limited to [-1,1]. What happens when one of the limit points is reached depends on the signal connected to the ADC. In the case of the pendulum- and armposition, it simply leaps to the other limit point. This can be seen in, for example, Figure 34. For the pendulum angle these limitations were not a problem. The breakpoint was just set at about $\pi/2$, an angle not normally used. For the armposition it is not desirable to have a breakpoint each lap, since the control of the arm may start at any angle. It has therefore been decided to have the breakpoint at about every eight laps. The arm may, therefore, run several laps before reaching a limit of the ADC. As a side-effect, the scaling factor for the armposition is greater than π.

To measure the scaling factor, the arm was rotated *exactly* one lap, during which the position of the arm was measured. The measurement was done using RT-Simnon, which was run in open loop. The result is shown in Figure 35. The data was analyzed using Matlab, and the position of the arm before and after the revolution were calculated. They were found to be $x_0 = -0.0699$ and $x_1 = -0.3132$. The difference between them is $x_0 - x_1 = -0.0699 - (-0.3132) = 0.2433$. Since one lap corresponds to 2π radians, the scaling factor between the real armposition Ω and the measured armposition x is $2\pi/0.2433 = 25.8$.

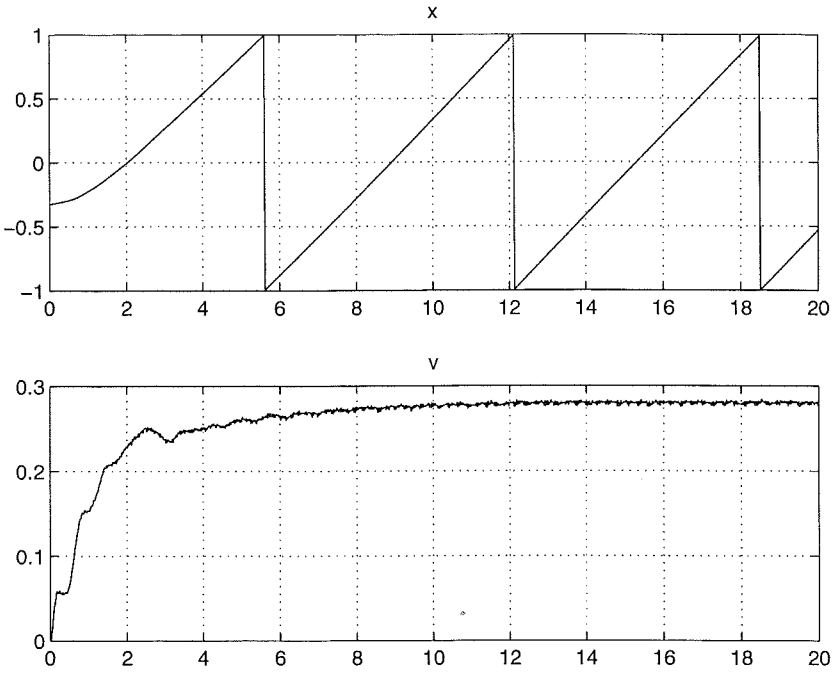

Figure 36 The velocity of the arm. The measured position is denoted by x, and the measured velocity is denoted by v.

As with the pendulum angle, the armposition has a bias x_0. The starting point of the control of the arm is defined as $\Omega = 0$. Since the control may start at an arbitrary angle, the bias x_0 is different every time the regulator is started, and cannot therefore be given a specific value. The bias is dynamic.

To summarize, the conversion formula between the measured armposition x and the real armposition Ω is

$$\Omega = 25.8(x - x_0) \quad x \in [-1, 1]$$

B.3 The Velocity of the Arm

The measurement of the scaling factor for the velocity of the arm requires a velocity controller. A simple P-regulator was used and it was implemented using RT-Simnon. The gain was set to $K = 0.15$ and the reference value was chosen as $v_{ref} = 0.5$. The position and velocity of the arm were measured and plotted. The result is shown in Figure 36. Both signals are unscaled. As can be seen, there is a stationary error in the control of the velocity on account that a P-regulator was used, but this is not any reason for concern since only the stationary velocity was used, not the reference value. Data from the experiment was analyzed using Matlab. The stationary velocity was estimated by calculating the mean value of a number of data points. The result was $v = 0.2801$.

To calculate the scaling factor, the actual velocity of the arm in rad/s was required. This could be estimated by for example counting the number of laps the arm did in, say, 30 s after having reached its stationary velocity. A more accurate way is to plot the position of the arm versus time and then measure the time it takes for the arm to go from -1 to 1. The result is shown in Figure 36. Using Matlab, the time was found to be 6.41 s. Since the scaling factor for the

arm position is 25.8, going from -1 to 1 corresponds to $2 \cdot 25.8 = 51.6$ rad. The actual velocity of the arm is then

$$\dot{\Omega} = \frac{2 \cdot 25.8}{6.41} = 8.05 \text{ rad/s}$$

This should correspond to the measured velocity from the ADC, $v = 0.2801$. The scaling factor therefore is $8.05/0.2801 = 28.7$.

The measurement of the arm velocity has a bias v_0, even though it is small. Estimating this bias is simple. The arm was kept still while the velocity was measured using RT-Simnon. The test was repeated a few times. The value of the bias varied, but stayed within the interval

$$v_0 \in [-0.009, -0.026]$$

A reasonable mean value of the bias is $v_0 = -0.02$.

To summarize, the relation between the measured velocity v and the actual velocity $\dot{\Omega}$ is

$$\dot{\Omega} = 28.7(v + 0.02) \quad v \in [-1, 1]$$

B.4 The Control Signal

The scaling factor for the control signal is the most difficult one to estimate. There are two reasons for this. First, the relation between the input voltage to the motor and the acceleration of the arm is not linear. Secondly, the friction in the arm has to be taken into account. A fairly good estimate of the Coulomb friction has to be known in order to calculate the *effective* control signal, i.e., the output control signal minus the friction.

Let u_{DA} denote the control signal sent to the DAC, and let u denote the theoretical control signal, i.e., the one in SI units calculated in the program. If k_u denotes the scaling factor, the relation between these two may be written

$$u_{DA} = k_u \cdot u$$

Introduce $u_{fr} = F_{fr}/m$, the Coulomb friction divided by the mass of the arm. It is assumed that u_{fr} is constant. From Appendix E, we know that a good estimate of it is $u_{fr} = 0.035$.

In the experiment that follows, the transfer function of the arm, Eq. (5), is used. It is rewritten using the variables introduced above.

$$\ddot{\Omega} = \frac{1}{0.21 k_u}(u_{DA} - u_{fr} \operatorname{sgn}(\dot{\Omega})) \tag{26}$$

The relation between the theoretical control signal u and the control signal sent to the DAC u_{DA} is not linear. Linearization will therefore be used. The experiment will be confined to those parameter ranges which are to be used in the control. Preliminary experiments have shown that the velocity of the arm is concentrated to the region from -3 rad/s to 3 rad/s and that u_{DA} is concentrated to -0.15 to 0.15.

If a constant control signal is sent to the DAC, the arm starts to accelerate. By measuring the acceleration $\ddot{\Omega}$ and then applying Eq. (26), $\hat{k}_u$ can be calculated. Four different control signals were used: u_{DA} = -0.05, -0.075, -0.1 and -0.2. The velocity of the arm, $\dot{\Omega}$ in rad/s, was plotted versus time, as shown in Figure 37. The accelerations in the range $\dot{\Omega} \in [0, 3]$ were estimated by fitting straight lines. Then Eq. (26) was applied and $\hat{k}_u$ was calculated. The results are shown in the table below.

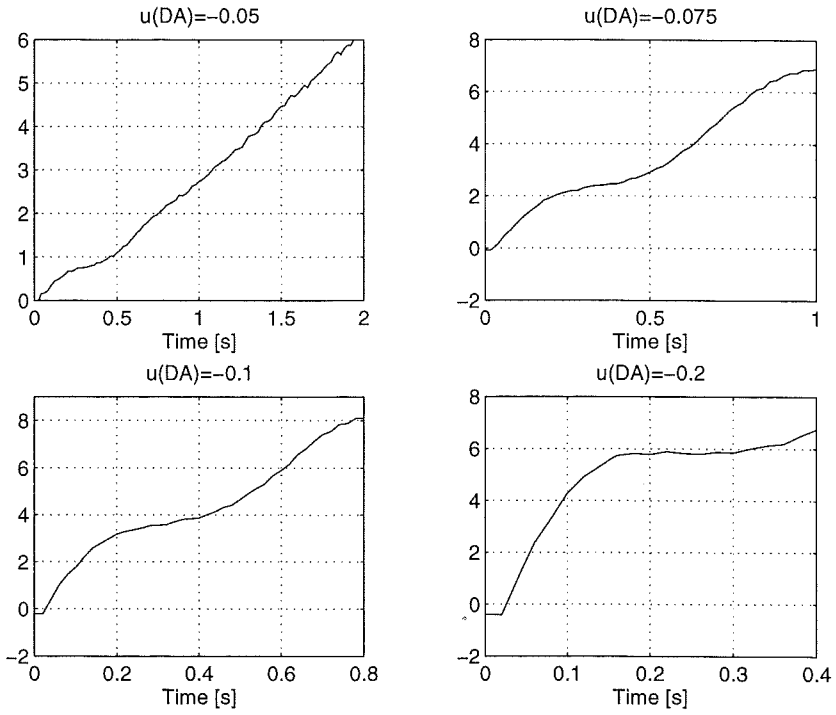

Figure 37 The control signal. Velocity of the arm versus time for u_{DA} = -0.05, -0.075, -0.1 and -0.2.

u	$\hat{\ddot{\Omega}}$	$\hat{k}_u$
-0.05	3.1	-0.023
-0.075	11	-0.018
-0.1	13	-0.024
-0.2	60	-0.013

As can be seen, $\hat{k}_u$ varies very much. Somewhat arbitrarily, the value $\hat{k}_u = -0.022$ was chosen.

Two remarks should be made. First, only negative control signals were used in obtaining $\hat{k}_u$. The reason is that these give rise to positive arm velocities and thus slightly nicer diagrams. It would have been more complete to also test what results positive control signals would give, but it was expected that the result would be about the same. The value $\hat{k}_u = -0.022$ was tested in practice and found to work well. Secondly, as can be seen in Figure 37 one gets some sort of plateau of constant velocity in each of the diagrams. When $u_{DA} = -0.05$ this is located around $\dot{\Omega} = 0.7$ rad/s, when $u_{DA} = -0.075$ it is about $\dot{\Omega} = 2.5$ rad/s, when $u_{DA} = -0.1$ it is about $\dot{\Omega} = 3.5$ rad/s and finally when $u_{DA} = -0.2$ it is slightly below $\dot{\Omega} = 6.0$ rad/s. I have no idea why this plateau arises and I have not investigated the matter further. Note, however, that in all three cases it seems to begin after about 0.2 s.

B.5 Summary

Here the scaling factors and biases for the input and output signals are sum-

marized. The denotations are explained in the text.

$$\begin{cases} \theta = \pi(y + 0.503) & y \in [-1, 1] \\ \Omega = 25.8(x - x_0) & x \in [-1, 1] \\ \dot{\Omega} = 28.7(v + 0.02) & v \in [-1, 1] \\ u_{DA} = -0.022u & u_{DA} \in [-1, 1] \end{cases}$$

C. Gains for the State Feedback Controller

Since the equations for the state feedback gains are large, they are not included in Section 2.2. Instead, they are given here. For denotations and explanations of the equations, see Section 2.2.

$$\begin{aligned} l_1 = &-\frac{1}{4}\big(4\cosh(\omega_0 h)^2 - 2\cosh(\omega_0 h) + 2p_2p_4\cosh(\omega_0 h) \\ &+ 2\cosh(\omega_0 h)p_1 + 2\cosh(\omega_0 h)p_3 - p_1 + p_2p_3 + p_1p_4 + p_4 - p_3 \\ &- 1 + p_2 - p_2p_4 + p_1p_3\big)g\Big/\big(\cosh(\omega_0 h)^2 - 2\cosh(\omega_0 h) + 1\big) \end{aligned}$$

$$\begin{aligned} l_2 = &-\frac{1}{4}\big(4\cosh(\omega_0 h)^2 + 2\cosh(\omega_0 h)p_1 + 2\cosh(\omega_0 h)p_3 \\ &+ 2\cosh(\omega_0 h) - 2p_2p_4\cosh(\omega_0 h) - p_2p_3 - 1 + p_4 - p_2p_4 + p_2 \\ &- p_1p_4 + p_1p_3 + p_1 + p_3\big)g\Big/\big((\cosh(\omega_0 h) - 1)\,\omega_0\sinh(\omega_0 h)\big) \end{aligned}$$

$$l_3 = -\frac{1}{2}\frac{(p_2p_3 + p_2 + p_1p_4 + 1 + p_1p_3 + p_2p_4 + p_4 + p_1 + p_3)L_1}{h^2\,(\cosh(\omega_0 h) - 1)}$$

$$l_4 = -\frac{1}{4}\frac{(5 + 3p_1 + 3p_3 + p_2 + p_4 - 3p_2p_4 + p_1p_3 - p_1p_4 - p_2p_3)L_1}{h\,(\cosh(\omega_0 h) - 1)}$$

D. Gains for the Two Control Designs

For use in the experiments in Sections 5 and 6, two control designs are introduced in Section 2.4. Pole configurations for the state feedback and for the Kalman filters are given there. In this appendix, the L- and K-vectors corresponding to these are given. The L-vector contains the gains for the state feedback loop, the K-vector contains the gains for the Kalman filters.

The gains for the fast design are

$$\begin{cases} l_1 = -86.6267 \\ l_2 = -11.8530 \\ l_3 = -19.7987 \\ l_4 = -6.89851 \end{cases}$$

and

$$\begin{cases} k_1 = 28 \\ k_2 = 65.6235 \\ k_3 = 0.07002 \\ k_4 = 0.48280 \end{cases}$$

The gains for the slow design are

$$\begin{cases} l_1 = -31.3510 \\ l_2 = -4.13566 \\ l_3 = -1.82609 \\ l_4 = -1.23275 \end{cases}$$

and

$$\begin{cases} k_1 = 28 \\ k_2 = 65.6235 \\ k_3 = 0.05251 \\ k_4 = 0.27396 \end{cases}$$

E. Simple Identification of Friction

Some simple friction experiments were performed on the inverted pendulum. First the stiction and the Coulomb friction were estimated. Then a rough Stribeck curve was determined.

E.1 Stiction and Coulomb Friction

Estimating the stiction is very simple. Constant control signals of increasing magnitude were sent to the DAC until the arm started to move. This gives the value of the stiction. The tests were made using RT-Simnon, and the stiction in both directions were estimated.

To determine the Coulomb friction the same method as in determining the stiction was used. The natural exception was that lower magnitudes of the control signals were used. Since the Coulomb friction is lower in magnitude than the stiction the arm had to be given a slight push to overcome the stiction. As is shown in the next subsection, the Coulomb friction, or more correctly the kinetic friction, varies with velocity and therefore depends on how hard the arm is pushed.

Although the experiments are simple to perform, accurate results are difficult to get. The reason is that the friction varies from time to time, and also differs depending on how much the inverted pendulum has been used before the tests. The latter is explained by the fact that the viscosity of the lubrication is high when the pendulum is started and then decreases after the pendulum has been run a while.

It was found that friction varied slightly depending on direction. For positive velocities, i.e., clockwise direction, the stiction was found to be

$$F_S^+ \in [0.045, 0.055]$$

and the Coulomb friction was mostly concentrated to the range

$$F_C^+ \in [0.035, 0.040]$$

Friction in the counterclockwise direction is slightly smaller, with

$$F_S^- \in [0.045, 0.050]$$

and

$$F_C^- \in [0.030, 0.035]$$

A few remarks should be made. The given friction values are magnitudes. In practice the friction for negative control signals is negative and vice versa. Also, the given values are the measured ones, i.e., they are unscaled. At the end of this subsection scaled parameters are given. It should once again be pointed out that friction varies with many factors and that one might get values of the friction parameters that are outside the given ranges. But they are good approximations of the real, "ideal world" intervals.

Since intervals are difficult to use practically and since the differences in the friction depending on direction are not very large, mean values for the parameters are given. A good estimation of the stiction is $F_S = 0.050$ and a good approximation of the Coulomb friction is $F_C = 0.035$. When translating these values to SI-units, i.e., when dividing them with $|k_u| = 0.022$, one gets $F_S = 2.3$ and $F_C = 1.6$.

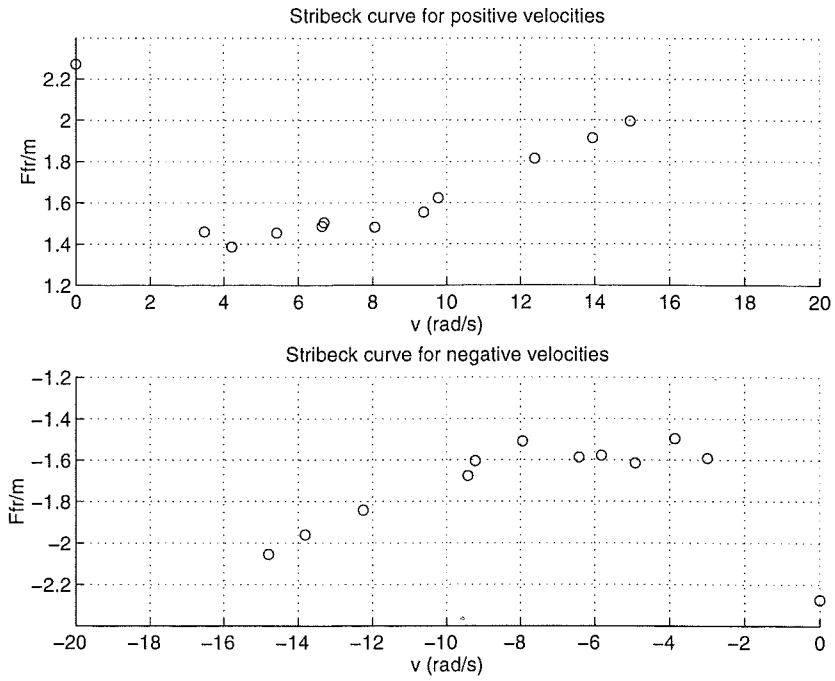

Figure 38 Stribeck curve for the inverted pendulum.

E.2 Stribeck Curve

The second simple experiment is designed in order to get the Stribeck curve. The test has two goals. The first is to determine to what extent a Coulomb friction model can be used, i.e., to see how flat the Stribeck curve is. Since the friction is determined in a different way than in the previous subsection the second goal is to verify the suggested mean value for the Coulomb friction.

The Stribeck curve was determined using RT-Simnon and a P-regulator to control the velocity of the arm. Different values of the gain and of the reference value were set. When the velocity had reached stationarity the values of the velocity and of the control signal were measured. Since the velocity is constant, the control signal should be zero. Because of the friction it is non-zero and its value is equal to the friction at the measured velocity. This can easily be seen in Eq. (5). Both positive and negative velocities were tested and the resulting Stribeck curves are shown in Figure 38. Velocities below ≈ 3 rad/s could not be examined with the method used. The results for larger velocities are not entirely reliable, since unwanted phenomena like air resistance affects the arm. But the experiments are not meant to be precise, they are only to serve as guidelines for the more advanced ones to come. What is significant in the diagrams is the shape of the curve and the mean value of the kinetic friction for lower velocities. The Stribeck effect is clearly visible, the curves are u-shaped. As for the goals of the test, the first one is fulfilled. The friction may be considered constant for low velocities. The second goal, that $F_C = 1.6$ is a good approximation for the magnitude of the Coulomb friction, is fulfilled for negative velocities but is a bit over the target for positive velocities. The value $F_C = 1.5$ would be more appropriate.

In the full fluid lubrication regime of the Stribeck curve the relation between friction force and velocity may approximately be considered linear. The slope of this line is called viscous friction and is denoted by F_v. This effect is

clearly visible in the Stribeck curve in Figure 38 for velocities above 10 rad/s in magnitude. By fitting straight lines to these points in the diagrams, an estimate of the viscous friction can be calculated. The result is $\hat{F}_v = 0.067$ in the case of positive velocites, and $\hat{F}_v = 0.075$ in the case of negative velocities. Since air resistance etc affected the measurements, the final estimate is given with one digit only: $\hat{F}_v = 0.07$.

Using Figure 38, an estimate of the Stribeck velocity v_S can also be calculated. This velocity affects the slope of the Stribeck curve in the boundary lubrication regime. Since no measurements are available in this regime, and since the exact value of v_S is not so very important, only its magnitude, $\hat{v}_S = 1$ rad/s was chosen as the estimate.

E.3 Summary

Two experiments were performed. First, the stiction and the Coulomb friction were determined by sending out constant control signals. It was found that the friction was slightly dependent on the direction of the arm. Secondly, a Stribeck curve was plotted using velocity control. Estimates of the stiction, the Coulomb friction, the viscous friction and the Stribeck velocity were calculated.

$$\begin{cases} F_S = 2.3 \\ F_C = 1.5 \\ F_v = 0.07 \\ v_S = 1 \end{cases}$$

F. Results from Simulation of the the LuGre Model

The tables below contain data from simulation experiments of the LuGre model. The fast control design was used. One parameter at a time was varied while the others were kept constant at their default values. The default values are given in Section 5.3. The denotations in the tables are explained in Table 1 in Section 5.1.

One remark should be made. The value $\sigma_0 = 100$ seems to be extremal regarding amplitudes and period.

F_S	peak1	peak2	valley	T	max(u)	max($\dot{\Omega}$)
1.9	0.201	0.184	0.182	0.892	8.2	3.9
2.1	0.205	0.187	0.185	0.888	8.5	4.1
2.3	0.209	0.190	0.187	0.884	8.9	4.2
2.5	0.214	0.195	0.190	0.877	9.2	4.3
2.7	0.217	0.198	0.192	0.872	9.5	4.4

F_C	peak1	peak2	valley	T	max(u)	max($\dot{\Omega}$)
1.1	0.183	0.165	0.160	0.866	7.8	3.6
1.3	0.195	0.178	0.173	0.878	8.4	3.9
1.5	0.209	0.190	0.188	0.883	8.9	4.2
1.7	0.221	0.204	0.200	0.887	9.4	4.5
1.9	0.233	0.214	0.209	0.895	9.9	4.8

F_v	peak1	peak2	valley	T	max(u)	max($\dot{\Omega}$)
0	0.203	0.183	0.179	0.863	8.5	4.0
0.07	0.209	0.190	0.188	0.883	8.9	4.2
0.14	0.215	0.199	0.196	0.902	9.2	4.4

v_S	peak1	peak2	valley	T	max(u)	max($\dot{\Omega}$)
0.5	0.199	0.183	0.182	0.890	8.1	3.9
1	0.209	0.190	0.188	0.883	8.9	4.2
2	0.219	0.200	0.194	0.875	9.5	4.5

Table 6 Variation of F_S, F_C, F_v and v_S.

σ_0	peak1	peak2	valley	T	max(u)	max($\dot{\Omega}$)
50	0.232	0.205	—	0.851	9.6	4.6
75	0.212	0.190	—	0.879	9.0	4.2
100	0.209	0.190	0.188	0.883	8.9	4.2
125	0.212	0.196	0.190	0.876	9.1	4.3
150	0.218	0.203	0.197	0.866	9.5	4.4
200	0.239	0.225	0.216	0.838	10.8	4.9

σ_1	peak1	peak2	valley	T	max(u)	max($\dot{\Omega}$)
0	0.198	0.158	—	0.936	7.3	3.7
3	0.201	0.176	0.175	0.907	8.0	3.9
5	0.209	0.190	0.188	0.883	8.9	4.2
7	0.224	0.209	0.202	0.851	10.0	4.6
10	0.261	0.249	0.240	0.795	12.3	5.6

k	peak1	peak2	valley	T	max(u)	max($\dot{\Omega}$)
0	0.183	0.157	0.153	0.963	7.1	3.5
0.01	0.184	0.157	0.153	0.959	7.2	3.5
0.1	0.185	0.159	0.156	0.956	7.3	3.6
1	0.209	0.190	0.188	0.883	8.9	4.2
2	0.303	0.288	0.281	0.747	14.3	6.5

Table 7 Variation of σ_0, σ_1 and k.

G. Table of Notation

The table below contains the most important denotations used in the report. Estimated variables have hats, for example, $\hat{\theta}$ denotes the estimated pendulum angle.

y	Measured pendulum angle (scaled and biased)
x	Measured arm position (scaled and biased), in Section 2: state variable
x_0	Bias of measured arm position
v	Measured arm velocity (scaled and biased)
u_{DA}	Control signal set out on the DAC (scaled)
$\theta, \dot{\theta}, \ddot{\theta}$	Angle, velocity and acceleration of the pendulum (rad, rad/s, rad/s^2)
$\Omega, \dot{\Omega}, \ddot{\Omega}$	Angle, velocity and acceleration of the arm (rad, rad/s, rad/s^2)
u	Control signal (m/s^2)
F	Generally: friction force, Section 2.1: tension (N)
F_{fr}	Section 2: friction force (N)
F_e	Externally applied force in the classical friction model (N)
F_C	Coulomb friction (N)
F_S	Stiction = static friction (N)
F_v	Viscous friction (N)
σ_0	Coefficient of stiffness in the LuGre model
σ_1	Coefficient of damping in the LuGre model
v_S	Stribeck velocity, in the LuGre model (m/s)
z	The state in the LuGre model (m)
ω_d	Damped natural frequency of the pendulum (rad/s^2)
ω_0	Natural frequency of the pendulum (rad/s^2)
ζ	Damping of the pendulum
L_1	Length of the arm (m)
L_2	Length of the pendulum (m)
ω_1	Desired natural frequency for the pendulum (rad/s^2)
ζ_1	Desired damping for the pendulum
ω_2	Desired natural frequency for the arm (rad/s^2)
ζ_2	Desired damping for the arm
ω_{o1}	Desired natural frequency for the pendulum in the Kalman filter (rad/s^2)
ζ_{o1}	Desired damping for the pendulum in the Kalman filter
ω_{o2}	Desired natural frequency for the arm in the Kalman filter (rad/s^2)
ζ_{o2}	Desired damping for the arm in the Kalman filter
k_u	Scaling factor for the control signal, between u_{DA} and u
g	Gravitational acceleration, 9.82 m/s^2
h	Sampling period (s)

H. References

ABELSON, C. F. and M. CHRISTELIUS (1996): "Identifiering av en inverterad pendel." Technical Report, Department of Automatic Control, Lund Institute of Technology, Lund, Sweden. Project report for the course System Identification.

ABELSON, C. F., M. DANIELSSON, and A. KARLSSON (1995): "Reglering av en inverterad pendel." Technical Report, Department of Automatic Control, Lund Institute of Technology, Lund, Sweden. Project report for the courses Adaptive Control and Real Time Systems.

CANUDAS DE WIT, C., H. OLSSON, K. J. ÅSTRÖM, and P. LISCHINSKY (1995): "A new model for control of systems with friction." *IEEE Trans. Automatic Control*, **40:3**, pp. 419–25.

EKER, J., E. GUSTAFSSON, and M. JOHANSSON (1996): "The rotating pendulum." Technical Report, Department of Automatic Control, Lund Institute of Technology, Lund, Sweden.

EKER, J. and K. J. ÅSTRÖM (1996): "A nonlinear observer for the inverted pendulum." In *Proceedings of the IEEE Conference on Control Applications, Dearborn, Michigan.* Department of Automatic Control, Lund Institute of Technology, Lund, Sweden.

KHALIL, H. K. (1992): *Nonlinear Systems.* Macmillan, New York.

OLSSON, H. (1996): *Control Systems with Friction.* PhD thesis, Department of Automatic Control, Lund Institute of Technology, Lund, Sweden.

SEARS, F. W., M. W. ZEMANSKY, and H. D. YOUNG (1987): *University Physics.* Addison-Wesley, seventh edition.

ÅSTRÖM, K. J. and B. WITTENMARK (1990): *Computer Controlled Systems. Theory and Design.* Prentice Hall, second edition.